**NASA CONTRACTOR REPORT** 166466



# Flow Analysis of Nozzle Installations With Strong Airplane Flow Interactions

D.W. Roberts


**CONTRACT NAS2**–10100
March 1983

NASA

**NASA CONTRACTOR REPORT** 166466

# Flow Analysis of Nozzle Installations With Strong Airplane Flow Interactions

Donald W. Roberta
Boeing Military Airplane Company
Seattle, Washington

Prepared for
Ames Research Center
Under Contract NAS2-10100

National Aeronautics and
Space Administration

**Ames Research Center**
Moffett Field, California 94035

TABLE OF CONTENTS

TABLE OF CONTENTS (CONT.)

## SUMMARY

A numerical procedure has been developed to calculate the flow fields resulting from the viscous-inviscid interactions that occur when a strong jet exhaust and aircraft flow field coupling exists. The approach used in the current procedure is to divide the interaction region into zones which are either predominantly viscous or inviscid. The flow in the inviscid zone, which surrounds most of the aircraft, is calculated using an existing linearized potential flow code. The viscous flow zone, which encompasses the jet plume, is modeled using a parabolized Navier-Stokes code. The key feature of the present procedure is the coupling of the zonal solutions such that sufficient information is transferred between the zones to preserve the effects of the interactions. The zonal boundaries overlap with the boundary conditions being the information link between zones. An iteration scheme iterates the coupled analysis until convergence has been obtained. The procedure has been successfully used for several test cases for which the computed results are presented.

# 1.0 INTRODUCTION

New varieties of military and commercial aircraft of interest use a strong coupling between the jet exhaust flow and the overall airplane flow field to enhance performance. These aircraft range from STOL transports such as the Boeing YC-14 and the NASA QSRA to combat aircraft with highly integrated nozzles that can be used for lift enhancement and thrust vectoring. Development of these aircraft requires the ability to achieve high performance for low development cost. The complex flow interactions characteristic of nozzle installations with strong flow field couplings make the development of such installations expensive, high risk undertakings when using conventional parametric test based design approaches. The 3-D flow fields associated with these installations can include mixing layers, wakes, separation, and strong curvature effects as illustrated in Fig. 1. With little applicable experimental data available and without appropriate analytical tools, the designer of such installations is faced with a formidable task.

In the traditional design approach, the designer relies heavily on parametric model scale wind tunnel test simulations of the proposed installation over the range of nozzle and flight conditions to be encountered by the aircraft. The available aerodynamic and propulsion performance data base is used to aid in the selection of a configuration. Analytical procedures used are generally 2-D and, therefore, have limited value. High quality model scale wind tunnel tests of complex nozzle installations have proven to be expensive and extremely difficult to implement. Often the details of the boundary layers and the jet plume are not measured. This leads to uncertain results which cannot be meaningfully scaled when designing a larger device. Hence, the test based design approach is usually expensive while providing results of unknown quality.

Developments in computational fluid mechanics and computer technology offer the potential for a significant improvement in the design process.

Numerical codes have been developed to model complex 3-D flows. When the appropriate analyses are available, parametric analysis can replace parametric wind tunnel testing in the design process. This offers distinct advantages since the analytical approach allows the designer to maintain precise control over the flow and boundary conditions. Full scale installations can be examined since physical size is not a constraint for a computer program. Furthermore, all of the flow variables can be examined in detail to obtain a better understanding of the flow. Wind tunnel testing is still necessary to validate the analysis and for "fine tuning" the design, but the configuration test matrix can be substantially reduced in size with an equivalent reduction in development cost. As computers increase in size and speed and codes become more efficient, the analytical approach offers an increasingly practical and less expensive alternative for the design process.

Analysis of the complex flow phenomena associated with the strongly coupled nozzle installations with a single flow analysis would require a solution of the complete Navier-Stokes equations. Even with today's flow modeling codes and state-of-the-art computers, this is not practical. Accurate numerical solutions would require vast amounts of storage and days of computer processing time. When the number of parameters to be varied in the design process is considered, one can imagine that the computational costs would be prohibitive aside from the necessary technology developments.

The problem of numerically modeling these complex flow fields can be examined from another perspective. Not all of the flow phenomena of interest occur in all regions of the flow domain. One can divide the flow domain into separate zones in which only certain phenomena are known to exist. The complete Navier-Stokes equations can then be simplified to model the flow in each zone. Hence, instead of one solution of the Navier-Stokes equations for the full domain, one has a set of simplified zonal solutions that must be carefully coupled together to preserve the interzonal interactions. This reduction in the overall complexity of the problem significantly decreases the computational costs and brings the

solution of the problem back into the realm of what is practical to achieve. The zonal modeling approach to the solution of fluid mechanics problems has existed for years. Numerous examples of procedures for successfully coupling potential flow codes to boundary-layer codes have been presented in the literature. These procedures have typically used a boundary-layer displacement thickness to couple the effect of the developing boundary layer to the potential flow solution. Lemmerman and Sonnad (Ref. 1) have recently demonstrated that a surface transpiration approach is equivalent while offering a reduction in computational costs. Brune, Rubbert, and Forester (Ref. 2) demonstrated a more sophisticated zonal modeling approach by coupling a potential flow code to a 2-D Navier-Stokes code to model the flow separation behind an ellipsoid. The demonstrated success of zonal modeling for these simpler flows suggests that it is a practical and feasible approach for simulating complex 3-D flow fields.

The objective of the work reported herein was to develop an analytical procedure for predicting strongly coupled jet exhaust interactions with the overall airplane flow field following a zonal modeling approach. In this analysis the flow domain is divided into inviscid and viscous zones. The inviscid zone encompasses the entire aircraft. The viscous zone is carved out of the inviscid zone and surrounds the jet exhaust plume which is dominated by viscous interactions. One can envision more zones such as the 3-D boundary layers on the aircraft surfaces or a separation zone on the nacelle as depicted in Fig. 1, but these are beyond the scope of the present study. In the inviscid zone, a 3-D potential flow solution is computed by the PANAIR pilot code (Ref. 3). A numerical method for the parabolized 3-D navier-Stokes equations (Ref. 4) is used to calculate the flow in the viscous zone. Key features of the present work are the development of a solution coupling procedure and an associated iteration scheme that result in converged solutions while preserving the necessary flow of information between the zones.

The following section presents a discussion of the individual codes. This is followed by a discussion of the coupling procedure. Next is a section in which the results of demonstration and validation test cases are presented. Finally, the concluding remarks and suggestions for improving the coupled analysis are presented.

## 2.0 DISCUSSION OF THE COMPONENT ANALYSES

To analyze the strong interactions between the jet plume and the flow field surrounding the aircraft, a procedure was developed to couple two existing codes. Each of these codes is particularly suited for predicting the flow characteristics in the zone in which it is used. The predominantly inviscid flow that encompasses the aircraft is predicted using the PANAIR pilot code. The flow in the jet plume is dominated by viscous effects which cause entrainment of the inviscid flow. The flow in this zone is calculated using a code that solves the parabolized Navier-Stokes equations. The analyses incorporated in these codes are discussed in the following sections.

### 2.1 PANAIR PILOT CODE

The PANAIR pilot code (henceforth called PANAIR) is a preliminary version of an advanced panel code intended to solve a variety of boundary value problems in steady subsonic or supersonic inviscid flow. This code is discussed in Reference 3. Just the subsonic capability will be considered here, since the coupled analysis procedure is at present limited to subsonic flow.

The PANAIR analysis is based on the assumption that for a wide range of flow conditions, a potential flow solution will substantially describe the flow past a prescribed configuration. This implies that the flow is assumed to be inviscid and irrotational.

The flow past the configuration is considered to be a small perturbation of a uniform flow that exists far upstream. PANAIR generates the potential flow solution in terms of the perturbation velocity potential, $\Phi$, which is used to calculate the local perturbations in the flow properties. The basic boundary condition employed in PANAIR is that the total mass flux vector be parallel to solid surfaces. Non-solid surfaces can have mass fluxes normal to the surface.

The method used in PANAIR to compute the potential flow is to superimpose fundamental solutions of the partial differential equation for $\Phi$. These fundamental solutions are sources and doublets whose locations are prescribed but whose strength must be determined to meet the prescribed boundary conditions. The sources and doublets are distributed on continuous networks of quadrilateral "panels" that approximate the surface of the configuration, as well as the vortex sheets shed from trailing edges and other surfaces such as inlet faces and jet plumes. Each panel is divided into subpanels on which the source and doublet strengths are approximated by linear and quadratic functions respectively. These functions contain the unknown source and doublet strengths which are then determined by the simultaneous solution of the algebraic system of equations. The resulting potential and velocity fields are then determined. The pressure field can then be calculated, and the forces and moments on the configuration can be computed.

### 2.1.1 Paneling

Although a detailed discussion of paneling concepts and problems is presented in Reference 3, some of the salient features are repeated here to emphasize the need for understanding the correct method for paneling a given configuration for use in the coupled analysis.

In general a configuration is divided into a system of networks which are composed of panels. The number of networks depends on the complexity of the configuration. The number of panels in a given network will depend upon the detail and accuracy desired from the analysis. To use PANAIR as part of the coupled analysis, networks for the surface of the configuration and its wakes must be supplied. Networks defining the jet plume and its wake are required. Additional networks are necessary for obtaining the flow properties at points off the body. These panels which do not disturb the flow, are specified with zero jumps in the potential and the normal component of mass flux.

The network surfaces are defined by an array of grid points which provide the coordinates for the corners of the quadrilateral panels. The array is

arranged in rows and columns. Care must be exercised in organizing these rows and columns since they, in effect, define the upper and lower surfaces for each network. Suitable diagnostics are provided by PANAIR to aide in debugging the network arrays. When networks abut, it is necessary that common grid points appear in all of the abutting network arrays. If the abutting networks have similar grid densities, the grid points used along the abuttment must be exactly the same in all of the arrays, unless one or more of the networks is free of doublets. This will insure that the doublet strength will be continuous at the network boundaries. Doublet networks must also abut along complete edges such that their network corner points coincide. This requirement often necessitates the division of a configuration into numerous small networks when junctures, such as between a wing and strut, are encountered. Failure to abide by the above rules will lead to disastrous results.

### 2.1.2 Boundary Conditions

The panels are covered with a continuous distribution of sources and doublets. Boundary conditions are imposed at selected "control points" on the networks to generate the necessary set of equations which are solved for the unknown singularity strengths. Networks can have just sources or just doublets in which case the boundary conditions for the other singularity type are not required. Special options exist for the treatment of wakes.

The user determines the flow behavior by specifying the types of boundary conditions on each of the networks. A great deal of flexibility exists, and Reference 3 describes the available options. The most commonly used types of boundary conditions are those for impermeable surfaces, the Morino-type boundary conditions. These are used on the wetted surfaces of an aircraft. For the coupled analysis the jet plume network has boundary conditions that allow the specification of the perturbation mass fluxes normal to the panel surfaces. Thus, the plume network is a permeable surface that entrains fluid from the surrounding potential flow. The use of this boundary condition is discussed in detail in Section 3.0.

### 2.1.3 Inputs and Outputs

The inputs to PANAIR are divided into four basic categories:

(1) General specifications
(2) Flow conditions
(3) Network geometry specifications
(4) Boundary condition specifications.

All of the inputs with the exception of the geometry are generally specified through FORTRAN coding in a special input subroutine. The geometry and part of the plume boundary conditions are provided in input files for the coupled analysis.

The outputs can be controlled to a large degree by the user. Options exist for printing out various types of diagnostics that allow a thorough examination of the health of the inputs before the solution routines are actually executed. Local aerodynamic data is always printed for every center-control point on every network. The output subroutine is modified for use in the coupled analysis to generate extra data files which transfer boundary conditions to the viscous zone.

## 2.2 PARABOLIZED NAVIER-STOKES CODE

The parabolized Navier-Stokes code (PNS) was developed to calculate a particular class of three-dimensional compressible viscous flows. The flows of interest are characterized by a predominant flow direction. In this class of flow, downstream disturbances have a negligible influence on the upstream flow. Thus, the assumption is made that the propagation of perturbations in the upstream direction by convection, diffusion, or pressure can be neglected for this particular class of flows. Cross stream propagation is allowed and in fact can be significant. Flows of this type are generally classified as being "parabolic". They exist in numerous internal and external flows ranging from complex 3-D duct flows to 3-D jets mixing with a freestream.

The time averaged Navier-Stokes equations with suitable closure for turbulent flows are acknowledged as being sufficient for analyzing complex viscous flow fields. When the above parabolic approximations are implemented, these equations are simplified so that they can be solved in a practical design oriented computer program. The Navier-Stokes equations are parabolized by neglecting the streamwise diffusion terms and decoupling the streamwise and cross stream pressure gradients. The streamwise pressure gradient is assumed to be uniform at each cross-sectional station. The resulting equations are elliptic in the cross stream and are often considered parabolic in the streamwise direction, however, this is more historical than formal. In the PNS code a simple marching solution procedure was implemented which eliminates communication with the downstream flow while solving the parabolized Navier-Stokes equations. Other features of the PNS code, which are discussed in the following sections, are the use of a general coordinate system, the transformation of the flow equations, the pressure-continuity relations, the turbulence model, the solution procedure, and the features that were added to automate the coupling with PANAIR.

### 2.2.1 General Coordinate System

Flows in geometrically complex domains are difficult to compute on standard orthogonal computational meshes such as Cartesian or cylindrical coordinate systems. The difficulties arise because the mesh points do not naturally fall on the boundaries of the flow domain of interest. This results in cumbersome differentiation and interpolation schemes at the boundaries that can achieve only low levels of accuracy. For many flows it is desirable to maintain high accuracy at the boundaries. For this reason significant effort in recent years (Refs. 5-8) has been aimed at generating general coordinate systems that are fitted to the boundaries of the flow domain. In the PNS code a curvilinear mesh is formed in which the boundary mesh points always fall on the natural boundaries of the flow domain and the interior mesh points conform to the boundary shape. This allows the use of standard differencing expressions and maintains high levels of accuracy at the boundaries. The boundary-fitted mesh is particularly suited for coupling with a panel method which also can handle

arbitrary geometries. Numerous methods exist for automatically generating the boundary-fitted meshes. These methods offer varying degrees of complexity and capability. Orthogonal meshes can be generated, but absolute orthogonality has not been demonstrated to be necessary or worth the effort, though highly skewed meshes are undesirable.

The boundary-fitted $\xi$, $\eta$, $\sigma$ coordinate system used in the PNS code can be generated using one of two options. The first method generates the interior mesh by simply interpolating between the inner and outer boundaries. This method has the capability of concentrating the mesh points near the outer boundary. The second method is similar to that discussed by Thompson, et al (Ref. 5). This method requires the solution of a coupled set of elliptic quasi-linear partial differential equations. A significant amount of flexibility exists since the interior mesh can be controlled by the use of suitable forcing functions. This ultimately allows one to automatically increase the mesh density in regions where greater accuracy is required. The 3-D mesh is generated in a step-by-step fashion. As the flow solution is marched from plane to plane the mesh at the next downstream plane is computed as the immediate precursor to the solution of the flow equations. Thus, the computational mesh for the complete flow domain only exists when the flow is completely predicted.

### 2.2.2 Transformed Flow Equations

To use the general boundary-fitted computational mesh, the flow equations are formulated with $\xi$, $\eta$, and $\sigma$ as the independent variables. Using standard transformation relations the Cartesian primitive variable form of the Navier-Stokes equations is transformed to the $\xi$, $\eta$, and $\sigma$ coordinate system. These equations are parabolized with the $\sigma$ coordinate specified to be the streamwise or predominant flow direction. The transformed equations are further simplified by requiring that the cross-sectional planes be parallel and perpendicular to the z coordinate. This limits the amount that the mean centerline of the flow domain can deflect from a straight line, but any significant curvature would typically indicate a non-parabolic flow. In $\xi$, $\eta$, and $\sigma$ coordinates the parabolized steady, three-dimensional continuity, momentum and energy equations are as follows:

$$(y_\eta \rho u)_\xi - (y_\xi \rho u)_\eta + (x_\xi \rho v)_\eta - (x_\eta \rho v)_\xi + (D\rho w)_\xi + (E\rho w)_\eta + [(J/z_\sigma)\rho w]_\sigma = 0 \qquad (1a)$$

$$Fu_\xi + Gu_\eta + (J\,\rho w/z_\sigma)u_\sigma + y_\eta P_\xi - y_\xi P_\eta = S \qquad (1b)$$

$$Fv_\xi + Gv_\eta + (J\,\rho w/z_\sigma)v_\sigma + x_\xi P_\eta - x_\eta P_\xi = S \qquad (1c)$$

$$Fw_\xi + Gw_\eta + (J\,\rho w/z_\sigma)w_\sigma + \frac{1}{z_\sigma}\overline{P}_\sigma = S \qquad (1d)$$

$$FH_\xi + GH_\eta + (J\,\rho w/z_\sigma)H_\sigma = S \qquad (1e)$$

where

$$D = \frac{x_\eta y_\sigma - x_\sigma y_\eta}{z_\sigma}, \qquad E = \frac{y_\xi x_\sigma - x_\xi y_\sigma}{z_\sigma}$$

$$F = y_\eta \rho u - x_\eta \rho v + D\,\rho w, \qquad G = -y_\xi \rho u + x_\xi \rho v + E\,\rho w$$

$$J = x_\xi y_\eta - x_\eta y_\xi$$

The appropriate diffusion terms, which are too cumbersome to present, are represented by the S on the righthand side of each equation. The Cartesian velocity components have been retained. The $\overline{P}_\sigma$ which appears in Eq. (1d) represents the constant streamwise pressure gradient for a given cross-section. In addition to the field equations, an equation of state is included, and a calorically perfect fluid is assumed. Sutherland's formula is used to relate the viscosity, $\mu$, to temperature.

### 2.2.3 Pressure-Continuity Relations

Although the streamwise and lateral pressure gradients have been decoupled to parabolize the flow equations, they are implicitly coupled through the continuity equation. The functional purpose of the pressure gradients is to insure the conservation of mass both globally and locally. Equations have been developed to guarantee this effect, since mass conservation is an essential requirement for the numerical simulation. A relation for $\overline{P}_\sigma$ is derived from the w-momentum equation and an integral definition for the mass flow rate in the diffuser. Mass is globally conserved by adjusting $\overline{P}_\sigma$ and iterating the w-momentum equation until the mass flow

rate reaches a specified level of accuracy. Global mass conservation is required before local conservation can be considered.

Local continuity is satisfied indirectly by means of the lateral pressure gradients $P_\xi$ and $P_\eta$. These pressure gradients are calculated such that the u and v velocity components generated by Eqs. (1b) and (1c) will simultaneously satisfy the continuity equation (1a) everywhere in the computational domain to a specified tolerance. The method used in the PNS code is similar to methods developed for time-dependent flows (Refs. 9,10).

Starting with a cell A in the lateral plane with vertices 1, 2, 3 and 4, an iteration scheme is developed. The u- and v-momentum equations indicate that a perturbation of the cell pressure has the following effect on the surrounding velocities.

$$u_i = \tilde{u}_i - \frac{1}{2}\frac{\Delta z}{J\rho w}(y_\eta - y_\xi)\Delta P_A \qquad (2a)$$

$$v_i = \tilde{v}_i - \frac{1}{2}\frac{\Delta z}{J\rho w}(x_\xi - x_\eta)\Delta P_A \qquad (2b)$$

$i = 1\text{-}4$

where the ~ represents the previous values. Equations (2) are substituted into the discrete form of the continuity equation (1a) to yield,

$$\Delta P_A = \omega \frac{C}{B} \qquad (3)$$

where C is the discrete continuity equation for cell A, B is a combination of mesh derivatives and velocity coefficients which result from the above substitution, and $\omega$ is an over-relaxation parameter. Using (3) $\Delta P_A$ is calculated. The surrounding velocities are then updated using equations (2) and the pressure $P_A$ is updated. This procedure is repeated at each computational cell. The computational plane is iterated until C decreases below a specified small value at all cells. A

relaxation factor of 1.5 seems to be optimal as long as the C distribution is relatively smooth; otherwise, slight under-relaxation is necessary until the smoothness develops. This pressure iteration scheme does not directly include the momentum convection and diffusion effects, however iteration with the momentum equations does implicitly produce these effects. Since iteration is already part of the solution procedure, no additional iteration is required.

### 2.2.4 Turbulence Model

Closure of the set of flow equations for turbulent flows is achieved by modeling the Reynolds stresses that appear in the time-averaged Navier-Stokes equations. In the PNS code these stresses are modeled by replacing the laminar viscosity $\mu$ with a turbulent eddy viscosity $\mu_\tau$. The eddy viscosity is calculated from the turbulence kinetic energy k and the turbulence kinetic energy dissipation rate $\varepsilon$.

$$\mu_\tau = C_\mu \rho k^2 / \varepsilon$$

The values for k and $\varepsilon$ are calculated using two additional transport equations (Ref. 11), which have the same form as Eq. (1e) with additional terms that model production and dissipation.

### 2.2.5 Boundary Conditions

The three velocity components u, v, and w are set to zero on walls. An adiabatic wall boundary condition is used with the energy equation. To minimize the mesh requirements in the lower regions of boundary layers, law-of-the-wall functions are used to represent the velocity distribution near the wall. These functions are used to calculate the wall shear stress and the production and dissipation source terms in the turbulence model equations for the wall region. The use of wall functions allows k and $\varepsilon$ to be accurately predicted in the vicinity of a wall.

### 2.2.6 Numerical Solution Procedure

All of the differential equations presented above have been transformed to finite-difference form by standard second order centered difference

approximations for $\xi$ and $\eta$ derivatives and by one-sided upstream differences for $\sigma$ derivatives. Since this makes the numerical approximation formally second order for a suitable streamwise step size, numerical noise can always be expected to generate spurious solutions that can be catastrophic unless it is properly controlled. A noise filter based on the work of Forester (Ref. 12) has been incorporated in the numerical algorithm to reduce the effects of the computational noise to negligible levels.

An iterative marching solution procedure was developed to allow converged numerical solutions after just one pass through the flow domain. An initial set of data is required at the starting plane. A solution is obtained at each successive cross section before a step is taken downstream to the next lateral plane. The solution of the nonlinear flow equations at each plane is achieved by an iterative ADI procedure. Iteration is required at each plane to reduce the accumulation of truncation errors that can result from linearization. Iteration allows a fully converged implicit solution at each plane. Usually, just a few iterations are required to achieve reasonable accuracy unless the flow is changing rapidly in the streamwise direction. The flow chart in Fig. 2 illustrates the basic solution procedure used in the PNS code.

### 2.2.7 Features Added for PANAIR Coupling

To facilitate a fully automatic iterative coupling procedure for the PNS code and PANAIR, it was necessary to add several capabilities to the PNS code. A routine was written to generate the panel networks that define the jet plume boundary and the boundaries of the viscous flow domain. The mass fluxes through the boundaries are calculated in an additional routine. A special procedure was developed to track the jet plume with the computational mesh such that the mesh could be used efficiently. The vorticity of the plume is monitored to locate the plume edge. With this known, the position of the mesh at the next state can be projected. This also ensures that the panels defining the plume can be positioned outside of the mixing region where viscous effects dominate.

### 2.2.8 Inputs and Outputs

The inputs to the PNS code can be divided into four categories:

(1) Controls and options for mesh generation
(2) Physical constants
(3) Boundary points for the mesh
(4) Initial conditions for the flow variables

The inputs are all read from a data file. The flow variables can be initialized internally for a few special cases, but they are generally read from the data file.

The main output to the program provides the calculated values for each of the flow variables at all mesh points. Diagnostic outputs are available to provide a more detailed history of the evolution of the flow. An output file can also be generated for use in computerized graphic displays.

# 3.0 COUPLING PROCEDURE

The interactions between the jet plume and the surrounding flow field can be correctly simulated by the proper coupling of the component analyses. It is not sufficient to run each code once in its separate zone. The codes must interact with each other in such a manner that the solution for the entire flow field is convergent and unique within the limits allowed by the algebra incorporated in the codes. Each code must provide information to the other code that adequately describes the physical processes being modeled in that zone. The PNS code, which calculates the jet plume development, must provide PANAIR with the effects of entrainment at the plume boundary. PANAIR must use this information and the other aerodynamic effects of the aircraft to calculate the potential flow field and in turn provide boundary conditions for the PNS code. The procedure developed for coupling PANAIR and the PNS code is discussed in the following sections.

## 3.1 OVERLAPPING COMPUTATIONAL ZONES

The domain in which the flow field is to be calculated is divided into computational zones for the individual codes. The inviscid zone is oriented to include all regions which can be adequately modeled by the PANAIR potential flow solution. The viscous zone is positioned to surround the jet plume where the viscous interactions are predicted by the PNS code. The location of the boundaries for these zones is a significant aspect of the coupling procedure.

Abutting the zones such that the boundaries are coincident does not provide the necessary flow of information for a convergent coupled analysis. Since both codes in effect solve boundary value problems, a specification of boundary conditions on the coincident boundaries would lead to unique solutions in each zone that are functions of those boundary conditions. Unless a priori knowledge of the flow properties on the boundaries was available, the flows predicted in each zone would not

necessarily bear any resemblance to the physical flow. New information that could be used to update boundary conditions would not be available since the solutions are boundary condition dependent and their boundary conditions are identical. Iteration is useless without new information. Hence, coincident boundaries lead to a coupled analysis that does not allow the codes to interact and exchange information and yields an iteration procedure that will not be reliably convergent.

These considerations led to the conclusion that for the proper coupling of these two codes, the boundaries of the computational zones cannot be coincident. Furthermore, the boundaries of each zone should be arranged such that the boundary conditions are dependent upon the solution in the neighboring zone. This allows the necessary transfer of information from one zone to another. In the present coupling procedure, this is accomplished by overlapping the zonal boundaries. This is illustrated in Fig. 3 for the simple case of an axisymmetric nozzle exhausting into a co-flowing freestream. Note that the boundaries of the viscous zone extend well past the edge of the jet plume and into the region that is inviscid flow. The inviscid zone boundaries extend into the viscous zone to a close proximity of the plume edge where the flow is still dominated by inviscid effects. The overlapping region is shared mutually by both zones. Therefore, the boundary conditions applied in the PANAIR code on the plume boundary can be derived from the flow properties calculated by the PNS code. Similarly, the boundary conditions for the viscous zone can be obtained from the PANAIR solution. The overlapping boundaries therefore provide the necessary communication link between the two zones that allows a converged coupled solution for the flow domain.

The solutions computed by PANAIR and the PNS code are consistent within their numerical accuracies for the overlapping region. If the flows under consideration are restricted to those that are parabolic, the $\overline{P}_\sigma$ term in the Equation (1d) will be negligible for external flows. By realizing that the flow in the overlapping region is effectively inviscid, the flow equations reduce to the Euler equations. This region is also irrotational since no mechanism is present to generate vorticity. In the overlapping

region the PNS code is actually solving the potential flow equation which is the fundamental equation of the PANAIR analysis. Therefore, the two solutions should be consistent in this region. Due to the various approximations incorporated into these two codes, exact consistency cannot be achieved, but the accuracy will be comparable to that obtained for the complete coupled solution. The overlapping region should be kept reasonably small, since it would be inefficient to have a large region in which the flow is in effect calculated twice.

## 3.2 BOUNDARY CONDITIONS

The specification of the boundary conditions on the overlapping boundaries is straightforward. The solution from the PNS code is used to calculate the perturbation mass flux through each of the panels that form the jet plume boundary network. This is accomplished by averaging the predicted velocity components and density on the corners of each panel and using the result to calculate the component of the mass flux vector that is normal to the panel. The array of perturbation mass fluxes is stored for access by the PANAIR code.

The boundary conditions for the PNS code are determined from the PANAIR solution in a similar manner. Special panel networks that do not disturb the flow are positioned in the inviscid zone to form the boundaries for the viscous zone. The predicted velocities on the panels are used to generate the boundary conditions for the PNS code. In the PNS code, these velocities are also used to compute the mass flux entering the viscous zone. The upstream boundary of the viscous zone, Fig. 3, forms the initial data plane for the PNS code. On that boundary, the panel velocities are used to calculate initial conditions, therefore, that region is initially irrotational.

## 3.3 MESH AND PANEL GENERATION

The generation of the panels on the overlapping boundaries is directly related to the generation of the computational mesh for the PNS code. All

other panels are directly input into PANAIR through the normal input procedure. Various options can be used to define the boundaries for the overlap region. Each of these options affects the method used for generating the mesh and panels. To facilitate the discussion of these options, consider the diagram in Fig. 3.

The outer boundary of the overlap region (and of the viscous zone) is designated to have a computational mesh index of J=N. The inner boundary of the overlap region (the plume boundary for the inviscid zone) has the index J=JNP. In the PNS analysis, the JNP mesh points are computationally like all other interior mesh points in the viscous zone. The correct usage of the coupled analysis requires that the JNP boundary lies beyond the edge of the viscous plume while not crossing the J=N boundary.

The simplest option for generating the N and JNP mesh points is to specify the N boundary points at the initial plane and project these points to each downstream plane such that all planes in the viscous zone will have identical boundary contours. The JNP points are specified at the initial plane on the edge of the plume and projected downstream with a given slope such that the JNP boundary expands. The panels on the N and JNP boundaries are constructed by using the mesh points on these boundaries as the corner points for the panels. The initial plane panels are similarly generated from the initial plane mesh points. This option has limited capabilities since the expanding JNP boundary could cross the N boundary at some point which would cause the PNS code to blow up. This problem is rectified by allowing the N boundary to expand with the same slope as the PNS boundary. The boundary slope must be large enough for JNP boundary to capture the plume and small enough to efficiently use the available computational mesh. Only simple plumes can be considered since the plume trajectory is limited to a narrow path.

The complexity of the shapes of the plumes to be calculated is enhanced by another option in which the N boundary mesh points are specified for the initial plane and for all succeeding downstream planes. The JNP points are specified in a like manner. The associated panels are generated as

discussed above. Clearly, this option requires that the user have some knowledge of the expected trajectory of the plume. This information is often available when the analysis is being used to parametrically examine a case for which some experimental data exists for similar flows. Care must be used in specifiying the JNP boundary to guarantee it surrounds the jet plume.

Another option was developed for the coupled analysis to automatically track the jet plume. At the initial plane the JNP boundary points are specified. The N boundary points are computed based on the JNP points and the number of mesh points one desires to have between JNP and N. At each of the downstream planes the JNP points are positioned using the vorticity in the most recent plane to locate the plume edge. This procedure involves calculating the vorticity at all points and determining where the vorticity approaches zero, which indicates the edge of the plume. This data is used to project the JNP points downstream to positions that will be outside of the plume. The maximum change in position can be controlled by specifying a maximum slope from upstream to downstream. The N boundary points are then calculated as before, and the panels are generated. This approach to generating the mesh is flexible since the boundaries of the viscous zone can move and distort with the plume. The viscous zone can then be compact and computationally efficient.

## 3.4 ITERATION PROCEDURE

One iteration of the solutions in the inviscid and viscous zones will generally not be sufficient to yield a converged solution for the total flow domain. The essential ingredient is the information transfer between the two zones. This is accomplished by repetitively updating the boundary conditions and generating new solutions. An iteration procedure was developed for the coupled analyses to automatically perform the necessary data manipulations and transfers without requiring interruptions by the user.

To start the iteration process, an initialization of the boundary conditions on the overlapping boundary of one of the zones is required. This is done by making an "educated" guess as to what the boundary values should be. The better the guess the fewer the number of iterations to reach convergence. The zone in which one chooses to initiate the iteration is not important, unless auxiliary information is available to yield a better estimate of the boundary conditions in one of the zones. If the viscous zone is the starting point, the velocity components on the initial plane and the outer boundaries must be provided. The freestream velocity components are often adequate for this initialization purpose. By starting with the inviscid zone, one is faced with the task of estimating the perturbation mass fluxes on the plume panel network. First the overlapping boundary networks must be constructed by executing the panel generation portion of the PNS code. Unless knowledge of the jet entrainment is available, the initial plume boundary fluxes can only be guessed. Using a constant flux is sufficient to start the iteration procedure.

As a demonstration of the iteration procedure, assume that the solution is started in the inviscid zone and refer to Fig. 4. The overlapping boundary panels are generated by the PNS code. Then the perturbation mass fluxes on the plume panel network are initialized. PANAIR is executed in the inviscid zone. The potential flow solution is used to calculate the boundary conditions for the viscous zone. The next step is the execution of the PNS code in the viscous zone. This will include the generation of new overlapping boundaries if the plume tracking capability is utilized. New values for the boundary conditions on the plume panel network are computed from the viscous zone solution. At this point these new boundary values can be compared with the old values. If a prescribed level of convergence is achieved, the iteration procedure can be terminated. Otherwise, the iteration loop will continue for a given number of iterations. The alternative of starting the solution in the viscous zone has the same iteration loop with the exception that the starting point would be the fourth step in Fig. 4 in which an initialization of the viscous zone boundary conditions is made.

# 4.0 VALIDATION CASES

To demonstrate and validate the usefulness of the coupled PNS and PANAIR codes, several test cases were set up and run. The main purpose of these tests was to demonstrate the coupling procedure and show that converged solutions can be achieved. In addition information about the behavior of the coupling procedure as the solutions iterate in the different zones could be obtained and used to understand and improve the existing procedure. While the accuracy of the overall solution depends on the accuracy obtainable by each code, the accuracy of the coupled codes can be validated to some level of satisfaction by comparing the computed solutions with existing experimental data when possible. The following cases provide a variety of the applications of the coupled analysis.

## 4.1 AXISYMMETRIC JET IN A FREESTREAM

The first test case, a subsonic axisymmetric jet in a freestream, was used primarily as an aid in the development of the coupling procedure. The simplicity of this case, see Fig. 3, was desirable since the effects of the coupling procedure and the overlapping boundary condition could be readily isolated. In addition experimental data and previous computational work were available for comparison. To minimize the computational costs, the symmetry of the case was used to limit the solution domain to half of the jet. In addition just five mesh points were used on the circumference of the jet, while 21 points were used radially. In the overlapping region seven mesh cells were used to separate the inner inviscid zone boundary from the outer viscous zone boundary. The plume tracking option was used to locate the plume edge by monitoring the vorticity. This guaranteed that the number of mesh cells in the jet plume would be the same at all stations since the mesh expands at the same rate as the plume. It also ensured that the panels generated for the plume network would be outside of the plume where the strong viscous interactions dominate.

The freestream for this case had a Mach number of M=0.2. The ratio of the jet core velocity to the freestream velocity was 2.17. In the jet, the initial velocity was given a constant value which gave the initial velocity profile in the viscous zone a top hat distribution. This type of distribution has large velocity gradients which typically give rise to computational noise. The noise filtering incorporated in the PNS code effectively controlled the noise in the initial regions of the viscous zone until the steep velocity profiles had diminished. The turbulence quantities were initialized with values that were empirically determined for developing free shear layers. A constant total temperature was used in the jet and freestream. The initial marching step size, $\Delta Z$, for the PNS code was equal to 0.25 of the initial jet radius. The step size was then gradually increased to a maximum of 1.25 initial jet diameters for one run and 2.5 diameters for another to examine the effect of step size. The coupled analysis was started by generating the panel networks in the overlapping region, initializing the perturbation mass flux on the plume network, and executing PANAIR in the inviscid zone. Then the zonal solutions and the overlapping boundary conditions were iterated using the automated coupling procedure.

Experimental data for the axisymmetric jet is available for the decay of the jet centerline velocity and the spreading rate of the jet. Rodi (Ref. 13) has also computed axisymmetric jets using a turbulence model like that incorporated in the PNS code.

The results computed for this case using the coupled PANAIR/PNS analysis are presented in Figs. 5 and 6. The centerline velocity decay is underpredicted, Fig. 5, when compared with the experimental data, but the spreading rate calculations, Fig. 6, compare more favorably. However, the present calculations are similar to Rodi's. Rodi concluded that the two-equation turbulence model was adequate for calculating the axisymmetric jet when the velocity ratio was large. However, he also found that the accuracy of the calculations is sensitive to initial conditions, mesh density, and step size. The sensitivity to $\Delta Z$ is confirmed by the present results.

Of greater importance was the information obtained about the coupling procedure. The plume tracking option is effective in minimizing the required amount of computational mesh by placing the mesh and panels in the proper locations. However, since the final plume boundary is not known until the coupled solution converges, the plume tracker, which calculates the new boundary as the solution is marched through the viscous zone, moves the boundary with each iteration of the PNS code. In effect the overlapping boundaries approach their final positions as the flow solution converges. This has a detrimental effect which tends to reduce the overall convergence rate. The boundary conditions for the viscous zone are calculated at the previous boundary positions, however, they are used in the PNS code with the new boundaries. The movement of the boundaries has associated area changes and normal velocity errors which lead to an error in the mass flux into the viscous zone. It is this small error in entrainment that tends to reduce the convergence rate. This effect is demonstrated in Fig. 7 which shows the convergence histories for the boundary conditions at several locations along the developing jet. At the upstream locations the convergence rate is substantially greater than at the downstream locations. When the plume tracking option was activated, a maximum allowable spreading rate for the plume edge was specified. In the initial region this maximum slope was achieved for several steps during each iteration through the viscous zone. Hence, the boundary did not move with iteration or affect the local convergence rate. Farther downstream the maximum slope was not achieved, the boundary moved during each iteration, and the convergence rate was reduced.

Convergence of the viscous zone outer boundary position is not required for convergence of the flow solution, but the plume boundary needs to be converged. To reduce the detrimental effect of a moving outer boundary, the standard plume tracking option could be modified to move this boundary for a couple of iterations until a rough position is found. Then the outer boundary should be frozen to allow a more rapid convergence of the flow solution.

A related point of interest is the effect of convergence on the streamwise pressure gradient term $\overline{P}_\sigma$. As discussed in section 2.2.3, $\overline{P}_\sigma$ is adjusted to satisfy overall continuity. For the axisymmetric jet, $\overline{P}_\sigma$ should always be zero. However, errors in the boundary conditions lead to an inconsistent mass flow rate which results in a nonzero $\overline{P}_\sigma$. As the solution converges these errors diminish and $\overline{P}_\sigma$ approaches zero at all streamwise stations.

## 4.2 AXISYMMETRIC JET OVER AN AIRFOIL

The main purpose for developing the present coupled analysis was to provide an analytical method for predicing the effect of the jet plume on the aerodynamics of a given aircraft configuration. In section 4.1 the coupled PANAIR/PNS analysis was demonstrated for a simple jet to provide convergent solutions with an accuracy that depends on the limitations of the component codes. Jets of substantially greater complexity could be examined at various angles of attack, but that would not provide additional insight into the jet/aircraft interaction problem. To test the coupled analysis for the interaction problem, a simple test case was set up for an axisymmetric jet positioned over an airfoil of constant cross section. This case provides a degree of flexibility since the jet position can be varied to determine whether the analysis predicts the expected trends.

A schematic diagram for this test case is depicted in Fig. 8. The axisymmetric nozzle of diameter, $D_n$, is positioned a height, h, above the airfoil. The leading edge of the airfoil and the nozzle exit plane coincide. The half span of the airfoil was $2.5D_n$. The initial conditions for the jet and the freestream conditions were identical to those discussed above for the isolated axisymmetric jet. The bilateral symmetry plane was used to simplify this problem. The plume tracking option was also used for this case. A fairly coarse computational mesh and panel network representation was used to conserve computer costs since only trends were to be predicted and no experimental data was available.

The coupled procedure was initiated in the inviscid zone with a PANAIR solution and then iterated. This case was run with the nozzle at three different heights above the airfoil.

The basic result obtained from this study was the net lift on the airfoil. The airfoil drag was not considered since the boundary layers were not part of this investigation and the jet was not allowed to scrub the wing. Fig. 9 presents a plot of the airfoil lift versus the height of the nozzle. The lift has been normalized by the lift of the airfoil without a jet present, and the nozzle height is normalized by the nozzle diameter. One can observe that the increase in lift is greatest when the nozzle is closest to the airfoil and the interaction is the strongest. The entrainment of the jet increases the circulation about the airfoil which enhances lift. Fig. 9 can only be used to observe trends since the actual increment in lift will be a function of the length of the airfoil among other things. However, the trends predicted by the coupled analysis agree with what is found experimentally. This offers encouragement for the continued use of this analysis.

The effect of the jet/airfoil interaction on the convergence of the coupled flow solution was substantial. The convergence history for the boundary conditions on the plume network panels closest to the airfoil surface is presented in Fig. 10, with h/D =0.9 the perturbation mass fluxes approach their final values smoothly and quickly in just three iterations. The convergence behavior was substantially different with h/D =0.775. The rate of convergence was still reasonable, but four iterations were necessary, and it appears that one more iteration may have been warranted. Part of this slowdown is attributed to the movement of the jet plume boundaries since the plume actually was deflected upwards and then downwards as it progressed over the airfoil. The stronger interaction at the lower height also affects convergence since the plume has a greater influence on the PANAIR solution for the airfoil which in turn has a large influence on the PNS solution for the plume. In general large perturbations reduce the rate of convergence, particularly when the plume axis must move to a converged position.

## 4.3 USB NOZZLE/WING

A case of practical interest is that of a rectangular nozzle blowing over the upper surface of a wing, see Fig. 11. This upper surface blowing (USB) type of nozzle has been successfully used in recent years on such aircraft as the Boeing C-14 and the NASA QSRA. In the present case the computed results are compared with the experimental investigation discussed in Reference 14.

As shown in Fig. 11 the nozzle exit plane is positioned approximately 0.32 of the wing chord, C, from the leading edge. The nozzle half width, $R_n$, is .21C. The half span of the wing is 6.4 $R_n$. Since the coordinates for the wing cross section were not available, they were estimated from a diagram in Reference 14. The angle of attack of the wing was set to zero; however, for the experimental data the wing had an angle of attack which is not known. Therefore, only qualitative comparisons with the data were attempted.

The flow properties were set up to simulate one of the experimental test conditions as closely as possible. The freestream Mach number was $M_\infty$=0.6. The freestream total pressure and total temperature were 1400 $lb/ft^2$ and $520^0R$. The velocity profile at the nozzle exit plane was calculated from the experimental total pressure surveys. The average total pressure in the nozzle was greater than the freestream. Part of the nozzle flow was slightly supersonic which is beyond the capability of the PNS code, however, most of the viscous zone was subsonic which allowed the PNS code to successfully generate a solution. The boundaries of the inviscid and viscous zones were fixed since the plume tracking option was not designed to work on a solid surface. The computational mesh in the viscous zone was too coarse to provide more than qualitative results.

The principle result from this test case is the effect of the nozzle on the pressure distribution on the upper surface of the wing. Since the wing was analyzed at zero angle of attack and the wing cross section was

just an estimate, the calculated pressure distribution did not resemble the experimental data, and a comparison would be of little value. The predicted trends on the other hand were identical to those found experimentally. Figure 12 provides the calculated chordwise pressure distribution at a position Y=1.8 $R_n$ from the nozzle centerline (PANAIR coordinates are used). The distribution for the wing alone and the wing/nozzle with the jet are shown. It is observed that with the jet the pressure drops below the wing alone curve at approximately X/C=0.2 and rises above it at X/C=0.6. Hence, the effect of the jet plume is to reduce the lift of the wing at the spanwise position between X/C of 0.2 and 0.6 and increase the lift beyond X/C of 0.6. This trend is exhibited in the experimental data including the points at which the curves cross (Fig. 16 in Reference 14). This favorable comparison offers encouragement for the potential of the coupled analysis. Since part of the nozzle flow is supersonic, the pressure distribution along the nozzle centerline at $Y/R_n=0$ cannot be accurately calculated. By modifying the method for calculating pressure in the PNS code, these supersonic regions could be predicted. In addition this case should be run again with denser computational meshes and panel networks to assess the effects of truncation errors.

### 4.4 623 V/STOL MODEL

The Grumman 623 V/STOL wind tunnel model has been extensively tested by NASA/Ames (Reference 16). The 623 model is a fighter-type configuration Fig. 13, with the nacelle integrated into the wing at the wing/body junction. The nozzle is an ADEN rectangular cross-section nozzle, Fig. 14, with the thrust deflector flap blended into the wing trailing edge. The inboard edge of this flap forms a juncture with the body when the deflector angle is $0^o$. The flap can be moved to deflect the exhaust plume to increase lift at low speeds and provide increased maneuverability for the vehicle. At zero deflection angle the exhaust plume positioned at the wing trailing edge can still provide increased lift at low freestream Mach numbers since the jet entrainment induces additional circulation about the wing.

The 623 model has been tested for free stream Mach numbers ranging from 0.4 to 0.9 and angles of attack of nominally $0^{o}$ to $13^{o}$. Cruise and combat variations of the ADEN nozzle were used. The thrust deflector angle ranged from $0^{o}$ to $20^{o}$. The experimental data consists primarily of pressure coefficient distributions on the wings, nacelles, and body and of force and moment measurements. Exhaust plume measurements were not obtained. Limited total pressure data were taken upstream of the nozzle throat, and a few static pressures were measured along the nozzle walls. The nozzle stagnation conditions were set to simulate: (1) no flow, (2) a flow through nacelle, and (3) a supersonic exhaust plume. Since the PNS code does not currently have the capability for calculating supersonic plumes, a limited number of the 623 model test cases can be of use for demonstrating the coupled analysis. However, it was felt that analyzing a complete aircraft configuration would be beneficial for understanding the coupling procedure. In addition, the 623 model had already been successfully paneled by NASA Ames. The paneled 623 model is shown in Figure 15. The sparseness of the panels was required for the case to run on the Ames CDC 7600 computer. The additional panels needed by the coupled analysis necessitated the use of the Boeing CRAY computer.

### 4.4.1 Internal Nozzle Flow Analysis

To obtain a complete set of flow conditions at the nozzle exit plane for use in the coupled analysis, the internal flow field for the nozzle was computed. By choosing the appropriate options in the PNS code, the boundary conditions are switched to model an impermeable, no-slip, adiabatic wall. In this mode the program has been used to successfully calculate numerous internal flows (Reference 4).

The 623 model ADEN nozzle has two basic throat configurations, cruise and combat. The combat configuration, which was used for the present calculations, has a larger throat area. The internal geometry of the nozzle, Fig. 16, starts with a circular cross-section downstream of a choke plate assembly. This is followed by a rapid transition to a rectangular cross-section. At this point the nozzle width is fixed, but the height varies through the throat section to the exit plane.

The initial flow conditions downstream of the choke plate are required as input to the PNS code in order to calculate the internal flow field for the nozzle. The only available measurements from the test data were the mass flow rate and the total temperature and total pressure, hence, certain assumptions about the initial flow field were made. Since the choke plate tends to remove irregularities in the flow, uniform profiles for velocity, temperature, and the turbulence quantities were assumed to exist at the initial plane. The average velocity and static pressure were calculated from the known flow conditions. Using this set of initial conditions and the adiabatic, no-slip wall boundary conditions, the PNS code was used to march the solution to the nozzle exit plane. At this point a file containing the calculated flow field data was saved to be used for the plume initial conditions when the coupled analysis was used for the external flow field. At present it is not possible to couple the internal flow to the external flow, since a fully elliptic viscous analysis would be required.

#### 4.4.2 External Flow Analysis

The paneling for the 623 model with the thrust deflector at zero degrees deflection angle was available from NASA Ames. Since the panels for other deflector angles were not available, the coupled analysis could not be run to demonstrate the effects of thrust deflection. However, the zero angle data could still be used for comparison with the numerical results.

##### 4.4.2.1 623 Model with No Nozzle Flow

In preparation for implementing the coupled analysis the paneled 623 model was analyzed using PANAIR alone. The experimental nozzle pressure ratio NPR, was 1.0 for this case, indicating that no air was flowing through the exhaust nozzles. This was modeled by covering the nozzle exit with a panel network having an impermeable boundary condition. The freestream Mach number was 0.6 and the angle of attack was zero degrees. The purpose of this baseline case was to determine the adequacy of the PANAIR solution in the regions of interest without the interactions caused by the jet plume. The PANAIR results were compared with the experimental data at the stations where $y$ = 0.11, 0.41, and 0.76 of the aircraft's semi-span

distance, b/2. Here, y is the PANAIR spanwise coordinate direction. These stations correspond to locations on the upper surfaces of the fuselage, nacelle and wing. For this and all other 623 model cases the wake panel networks were angled up at five degrees.

The pressure coefficient, $C_p$, distribution along the upper fuselage station is provided in Fig. 17. Clearly, the PANAIR solutions follows the experimental data reasonably well. The most significant discrepancies occur on the aft 20 percent of the fuselage. In this region the boundary layer could be thick making separation a possibility, which would account for the substantial differences. The boundary layer at this station was not investigated experimentally. The other discrepancies may be associated with an insufficient number of panels to provide adequate resolution or with bad data points.

The results for the nacelle upper surface are shown in Fig. 18. The discrepancies between the PANAIR solution and the experimental data at this station are significant only at locations between 60 and 80 percent of the nacelle length, where the predictions seem to be out of phase, and at the leading edge. These differences are probably related to a lack of panels and viscous effects.

The wing $C_p$ distributions are compared in Fig. 19. The agreement between the analysis and experimental data is good except in the vicinity of the leading edge. This again may be due to an inadequate number of panels to resolve this region of strong acceleration.

Overall, the PANAIR solution for this non-flowing nozzle case seems to provide reasonably accurate results. Similar results were obtained at NASA-Ames using the same paneling. By increasing the panel density, better agreement with the experimental data may be obtained, but that is beyond the scope of this investigation.

4.4.2.2 623 Model With Flow Through Nacelle

The 623 model was tested at nozzle total pressures approximately equal to the freestream total pressure. This had the effect of simulating a flow through nacelle since the nozzle flow total temperature was equal to that in the freestream. The NPR for this case was 1.22. The freestream Mach number and angle of attack were 0.6 and $0^{o}$, respectively. Although the effect of the plume is small, the test data indicates it is noticeable, Fig. 20. Before this case could be analyzed using the coupled PANAIR and PNS codes, several modifications to the paneled 623 model were necessary.

Since the plume was exiting the nozzle at a low pressure ratio, it would not expand. The analysis from Section 4.4.1 was used to calculate the exit velocity profile, which had a mean value near the freestream velocity as expected. The lack of a significant velocity ratio between the freestream and the plume suggests that virtually no mixing would take place on the deflector ramp. In view of this the ramp was modified by enclosing it with panels that had the effect of moving the nozzle exit to the deflector trailing edge. This greatly simplified the complexity of the coupling precedure.

A further modification to the nozzle was required in order to accommodate the overlapping boundaries of the coupled analysis. Since the edge of the deflector flap in the $0^{o}$ position has a juncture with the fuselage, part of the overlapping mesh needed by the PNS code at the initial plane would be positioned inside the aircraft. This unallowable situation was remedied by adding a short impermeable extension to the nozzle. Since the aft end of the fuselage rapidly converges, a one inch extension was sufficient for the mesh boundaries to avoid the body. Though the extension does modify the plume flow slightly, the negligible expansion and mixing in this region make the effect insignificant.

The initial plume flow conditions for the PNS code were calculated as discussed in Section 4.4.1. The initial velocity profile had a peak value that was below the local external flow field. Therefore, this simulated flow through nacelle plume becomes a wake that interacts with the aircraft flow field.

The panels that define the nozzle trailing edge extension were modeled using just sources as opposed to the source/doublet panels used on the aircraft body. This was done to avoid problems associated with the requirement for a continuous doublet distribution at the intersection of the trailing edge wake panels with the deflector flap. The panels generated by the PNS code to define the plume were also specified to be pure source panels.

The coupled analysis was initiated by using the PNS code to generate the plume shape and associated panels. A uniform perturbation mass flux was specified on the plume for the first iteration of PANAIR. Each code was iterated four times, which was sufficient for convergence. Each iteration of the PNS code resulted in a new set of plume panels and mass flux distribution. After each iteration of both codes the results were examined before the next iteration was allowed to proceed. Convergence of the overall solution for this case was monitored by plotting the $C_p$ distributions for each iteration at the fuselage, nacelle, and wing stations. These distributions seemed to rapidly converge.

The results for this case are presented in Figure 21-23. The predicted $C_p$ distributions show the same trends as the experimental data. The incremental change in $C_p$ is greater for the coupled analysis solution along the aft half of the fuselage and nacelle. The $C_p$ distribution along the wing shows a favorable comparison between the analytical and experimental data. The agreement is particularly good along the aft end of the wing. The overall solution appears to be modeling the effect of the plume on the aerodynamics of the aircraft reasonably well.

4.4.2.3 623 Model with Jet Plume

Test data for cases with a jet plume were taken at nozzle pressure ratios that make the jet supersonic. Since the PNS code was not designed for supersonic flow, a case was set up for a plume with the initial Mach number set to 0.95. The intent of this case was to determine whether a jet could have a strong effect. A uniform velocity distribution at the exit plane was used. The ratio of the jet velocity to the freestream was

1.55. The total temperature and static pressure were the same as for the previous case. Four iterations of the coupled analysis were run for this case.

The predicted results for this case are shown in Figures 24-26. Clearly, the increase in $C_p$ is minimal. This is not totally unexpected. The low velocity ratio does not lead to significant mixing of the plume with the surrounding flow, which means that the entrainment effects should be small. At the relatively high freestream Mach number of this case, the effects of entrainment cannot be felt upstream as they are for low speed flows. An examination of the test data for the high NPR cases reveals the same trend demonstrated with the analysis. The small increase in $C_p$ with increasing NPR demonstrates that the coupled analysis procedure allows the jet entrainment effects to be calculated by the PNS code and transmitted to the PANAIR code through the overlapping boundaries. Test data with larger influences from jet entrainment on the wing circulation would be preferable for better analysis validation.

# 5.0 FUTURE WORK

As a result of the work discussed in this report and the need for advanced numerical procedures, several recommendations for future work are presented in this section. These recommendations are aimed at increasing the generality and efficiency of the present coupled analysis. Extending the analysis to allow the prediction of more complex flows can be pursued within this framework as more powerful analyses become available.

## 5.1 IMPROVEMENTS TO THE PRESENT COUPLING PROCEDURE

The present coupled procedure is still expensive for flow field solutions which require a substantial number of iterations for convergence. Methods for improving the convergence rate need to be investigated. The plume tracking option needs further development to include a provision for freezing the outer viscous zone boundary after the general plume location is established. This would stop the introduction of mass flux errors at the boundary that impede convergence. Panel and mesh density studies can then be accomplished more efficiently.

## 5.2 SUPERSONIC VISCOUS JET ANALYSIS

As discussed in Section 4.3, the PNS code will not accurately predict supersonic flows. However, nozzles with supercritical pressure ratios are often encountered, and it is desirable to have the capability to predict the supersonic jet plumes. The PNS code can be modified to implement pressure relations that are valid for supersonic flows. This would have to be done such that the resultant analysis is still compatible with the overall coupling procedure.

# 6.0 CONCLUSIONS

The most significant conclusion of the work discussed in this report is that a successful procedure has been developed for coupling PANAIR and parabolized Navier-Stokes solutions to allow numerical simulations of the strong interactions between jet plumes and the overall aerodyamics of aircraft configurations. Overlapping inviscid and viscous computational zones provide the means for information transfer between the solutions. The coupling procedure is automated and yields convergent solutions. This zonal procedure was applied to four test cases; an axisymmetric jet in a co-flowing stream; an axisymmetric jet above an airfoil; a rectangular jet on an airfoil; and a V/STOL fighter airplane configuration with 2-D nozzles at the wing trailing edge. Good quantitative agreement with experiment data was obtained for the first case. For the remaining cases, qualitative agreement was obtained. Computed results to date indicate that the panel densities for the PANAIR solutions and the mesh densities for the Navier-Stokes solutions significantly affect the predictions. Additional mesh refinement studies need to be performed to evaluate the procedure and to establish panel and mesh density criteria.

Both of the component analyses are limited as to the types of flows that can be simulated. The present coupling procedure can be extended by modifying the existing analyses and adding new analyses. The complexity of the flows to be predicted will determine which extensions need to the made. The technology developed for the present procedure will be directly applicable to future work.

## 7.0 REFERENCES


1. Lemmerman, L. A. and Sonnad, V. R., "Three-Dimensional Viscous-Inviscid Coupling Using Surface Transpiration," Journal of Aircraft, Vol. 16, No. 6, June 1979, pp. 353.

2. Brune, G. N., Rubbert, P. E., and Forester, C. K., "The Analysis of Flow Fields wth Separation by Numerical Matching," Symposium on Flow Separation, AGARD Fluid Dynamics Panel, 27-30 May 1975, Gottingen, Federal Republic of Germany.

3. Moran, J., Tinoco, E. N., and Johnson, F. T., "User's Manual Subsonic/Supersonic Advanced Panel Pilot Code," NASA CR-152047, February 1978.

4. Roberts, D. W., and Forester, C. K., "Numerical Prediction of Three-Dimensional Subsonic Diffuser Flows," Flow in Primary, Non-Rotating Passages in Turbomachines, American Society of Mechanical Engineers, New York, N.Y., 1979.

5. Thompson, J. F., Thames, F. C., and Mastin, C. W., "Automatic Numerical Generation of Body-Fitted Curvilinear Coordinate System for Field Containing Any Number of Arbitrary Two-Dimensional Bodies," Journal of Computational Physics, 15, pp. 299-319, 1974.

6. Smith, R. E. and Weigel, B. C., "Analytic and Approximate Boundary-Fitted Coordinate Systems for Fluid Flow Simulations," AIAA Paper No. 80-0192, January 1980.

7. Chen, L. T. and Caughey, D. A., "Transonic Inlet Flow Calculations using a General Grid-Generation Scheme," Flow in Primary, Non-Rotating Passages in Turbomachines, American Society of Mechanical Engineers, New York, N.Y. 1979.

8. Sorenson, R. L. and Steger, J. L., "Simplified Clustering of Nonorthogonal Grids Generated by Elliptic Partial Differential Equations," NASA TM-73252, August 1977.

9. Amsden, A. A., and Hirt, C. W., "YAQUI: An Arbitrary Lagrangian-Eulerian Computer Program for Fluid Flow at All Speeds," LA-5100, Los Alamos Scientific Laboratory, March 1973.

10. Pracht, W. E., "Calculating Three-Dimensional Fluid Flows at all Speeds with an Eulerian-Lagrangian Computing Mesh," Journal of Computation Physics, 17, 132-159, 1975.

11. Launder, B. and Spalding, D. B., "The Numerical Computation of Turbulent Flows," Computer Methods in Applied Mechanics and Engineering, 3, 269-289, 1974.

12. Forester, C. K., "Higher Order Monotonic Convective Difference Schemes," Journal of Computational Physics, 23, No. 1, 1977.

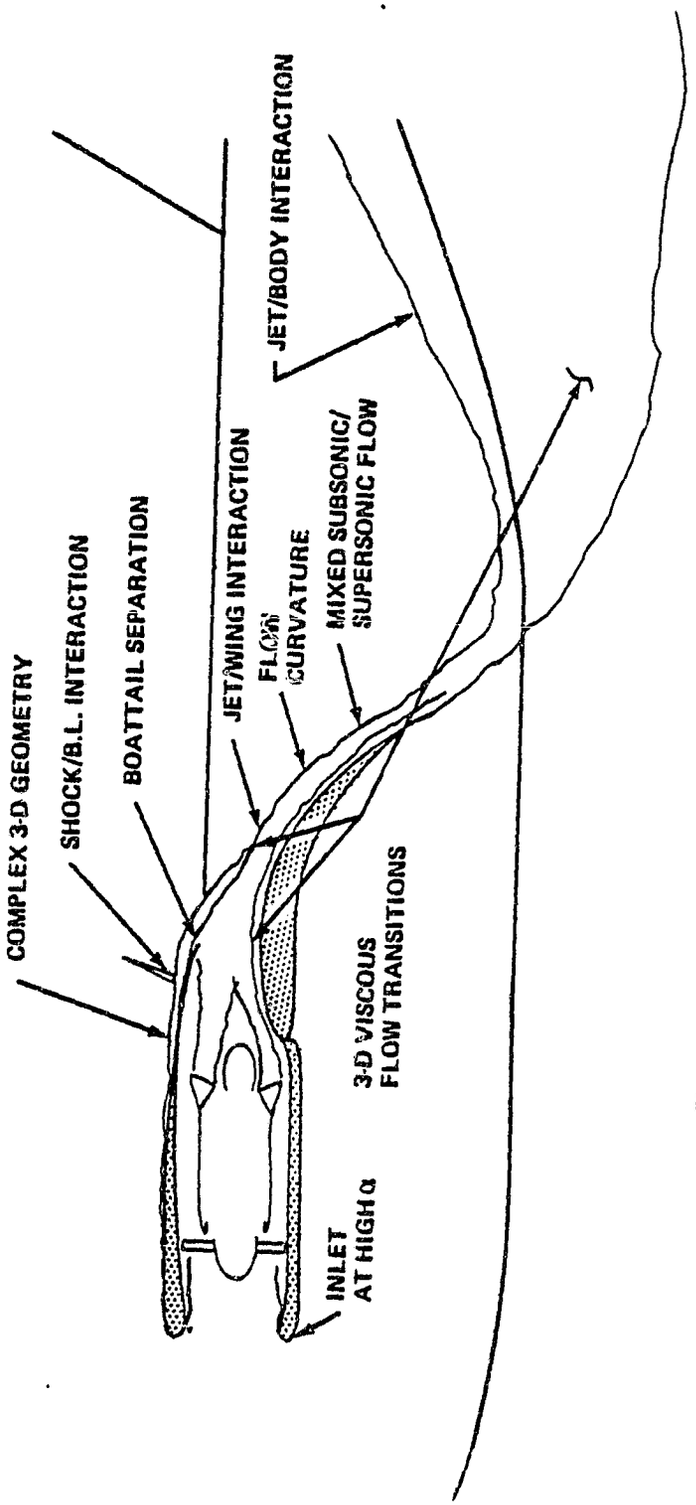


*Figure 1. Fluid Flow Problems of Propulsion Powered Lift Installations*

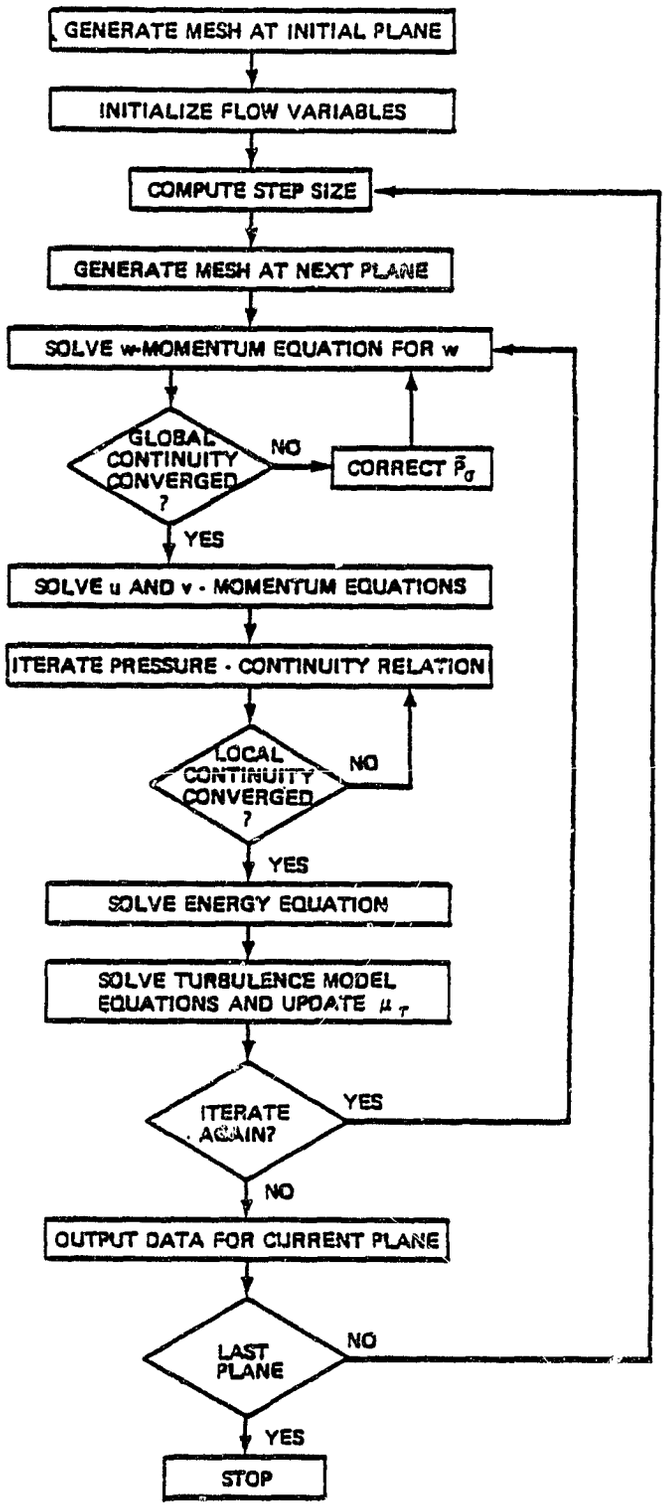


*Figure 2. Flow Chart for PNS Code.*

ORIGINAL PAGE IS
OF POOR QUALITY

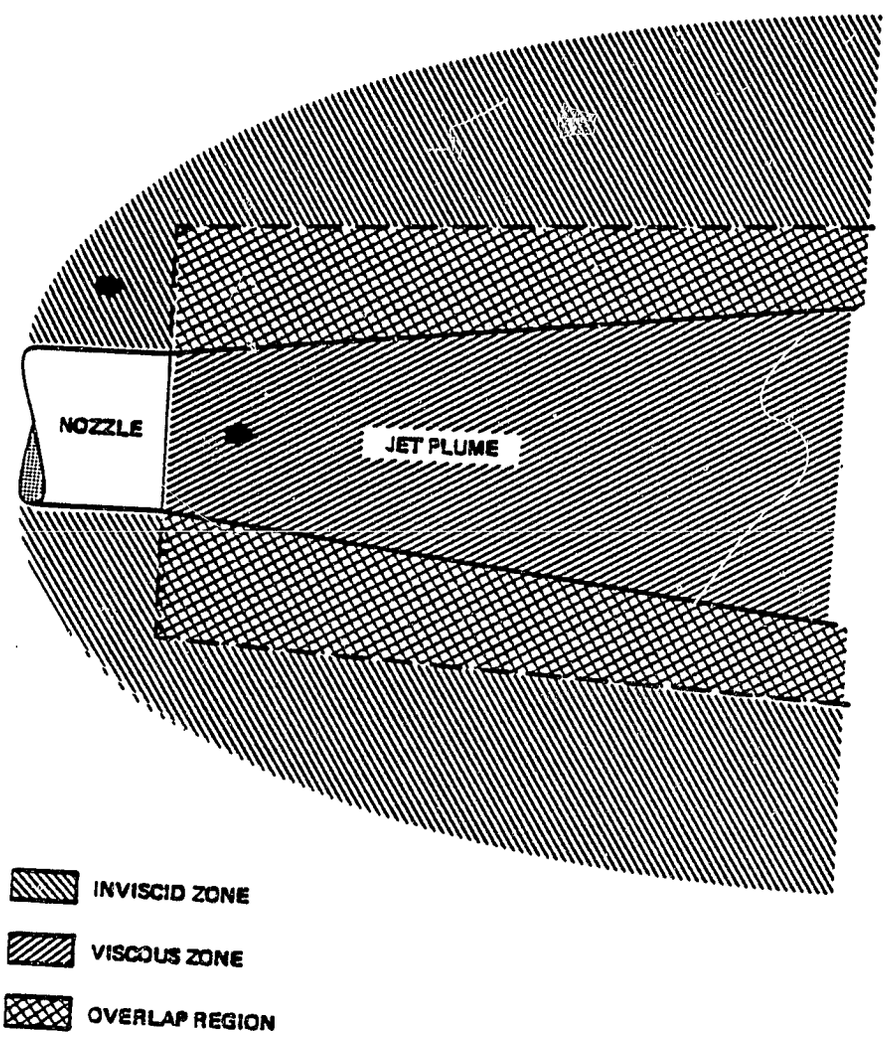


*Figure 3. Overlapping Zonal Boundaries*

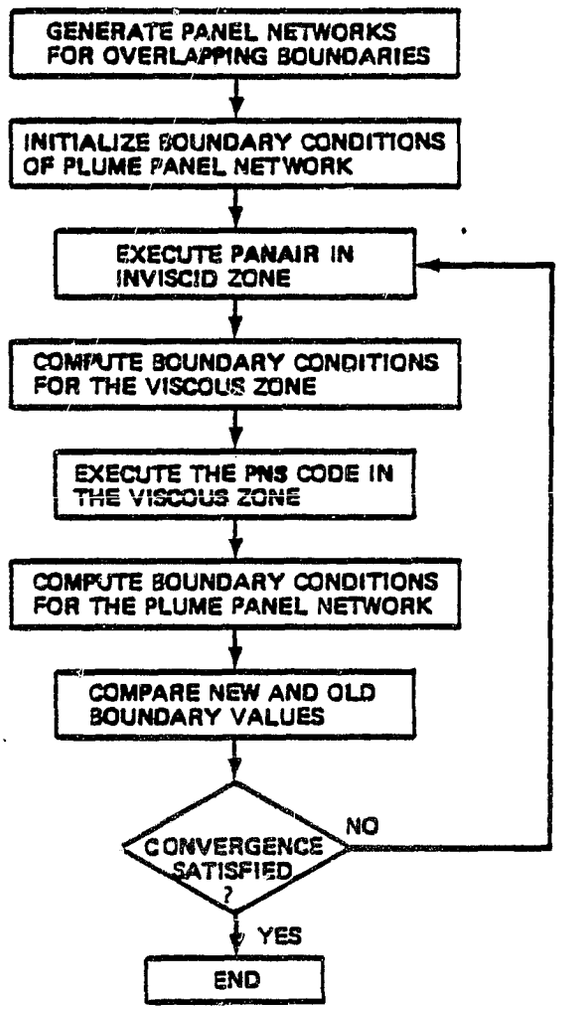


*Figure 4. Flow Chart of the Iteration Procedure Used in the Coupled Analysis*

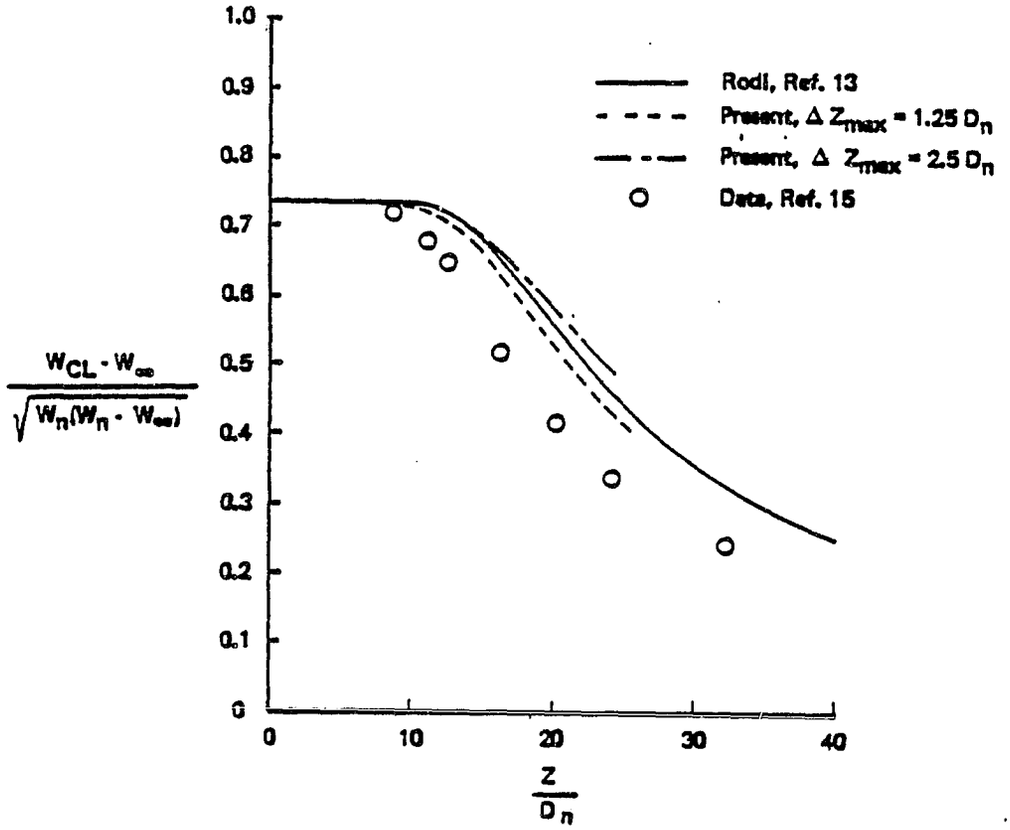


*Figure 5. Centerline Velocity Decay for Axisymmetric Jet*

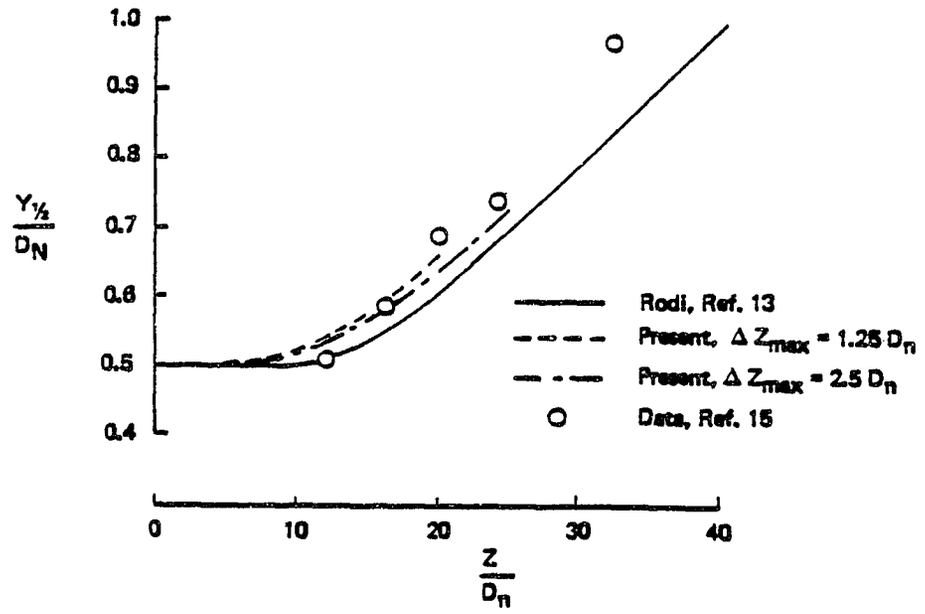


*Figure 6. Axisymmetric Jet Spreading Rate*

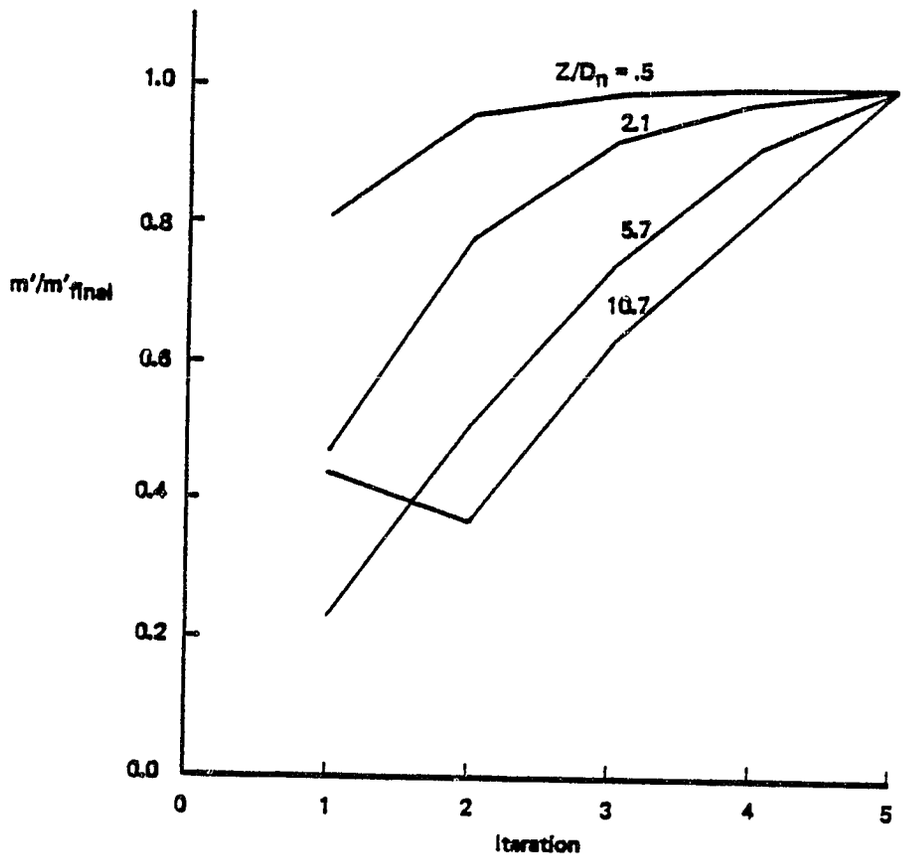


*Figure 7. Convergence Rate for Axisymmetric Nozzle*

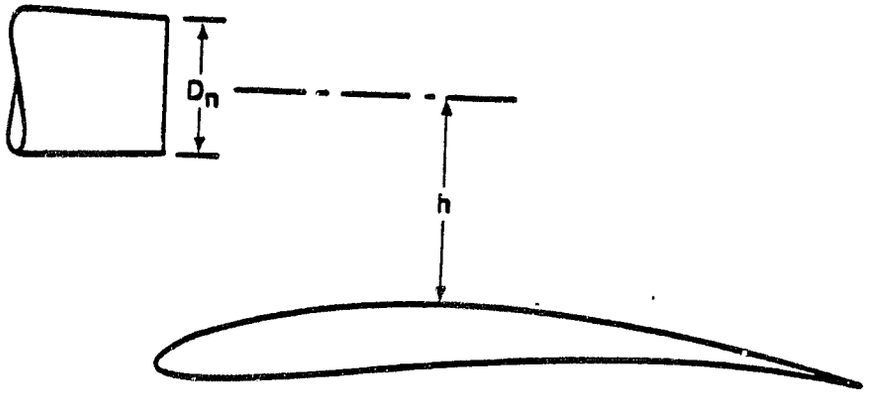


*Figure 8. Axisymmetric Nozzle Over an Airfoil*

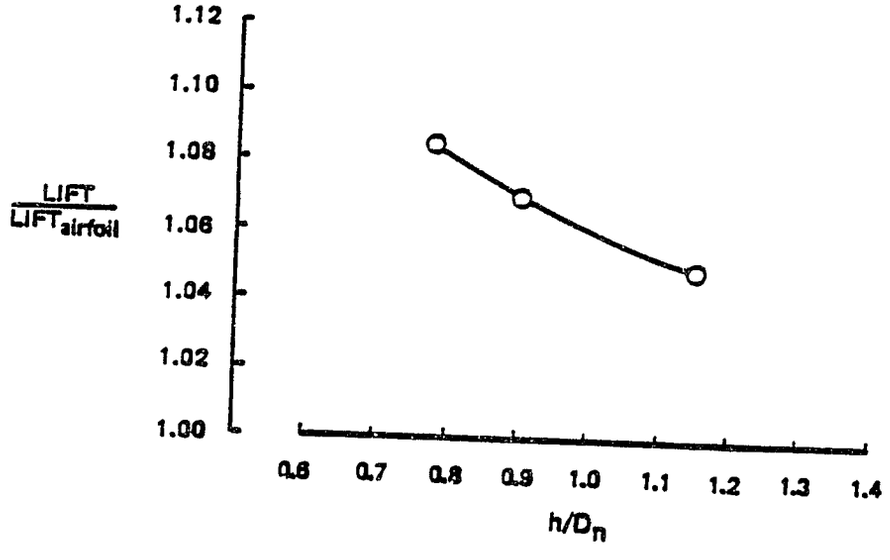


*Figure 9. Effect of Nozzle Height on Airfoil Lift*

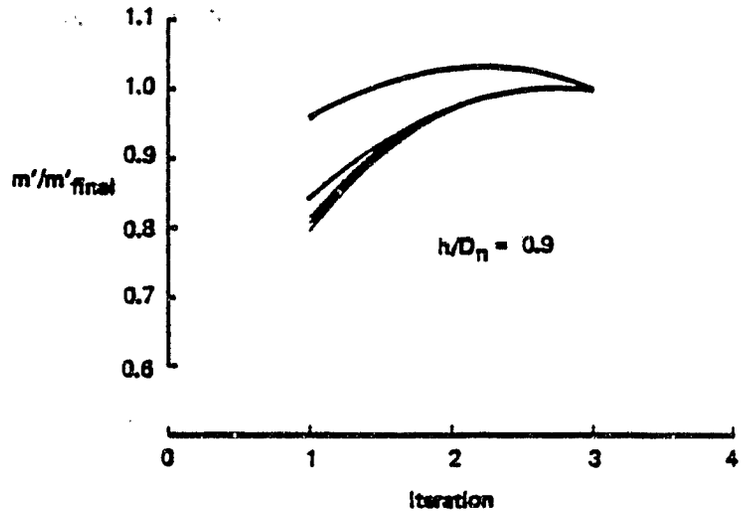


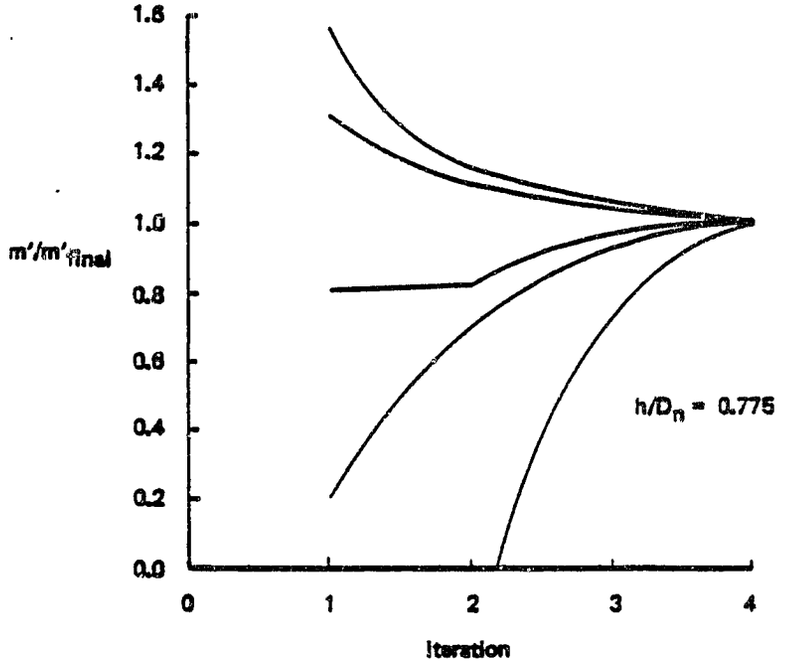


*Figure 10. Convergence History for Axisymmetric Nozzle Over an Airfoil*

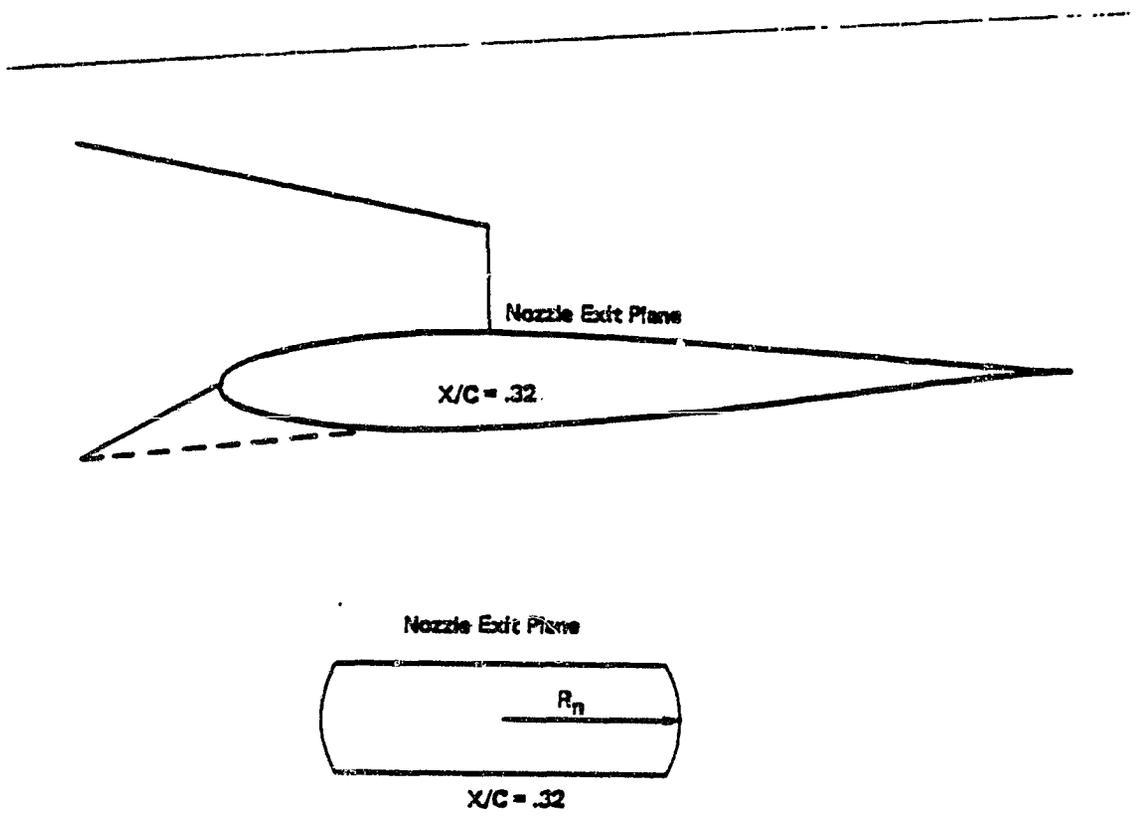


*Figure 11. USB Nozzle and Wing*

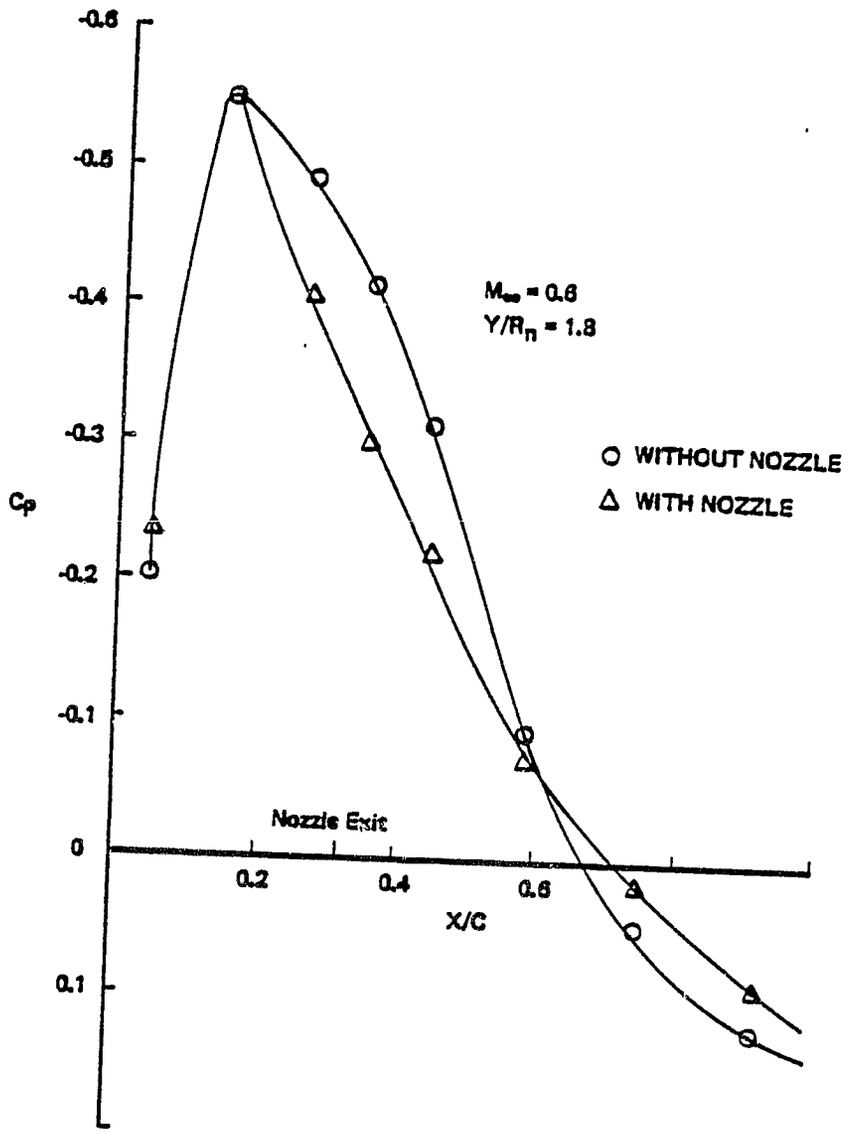


*Figure 12. Effect of Blowing Nozzle on Wing Pressures*

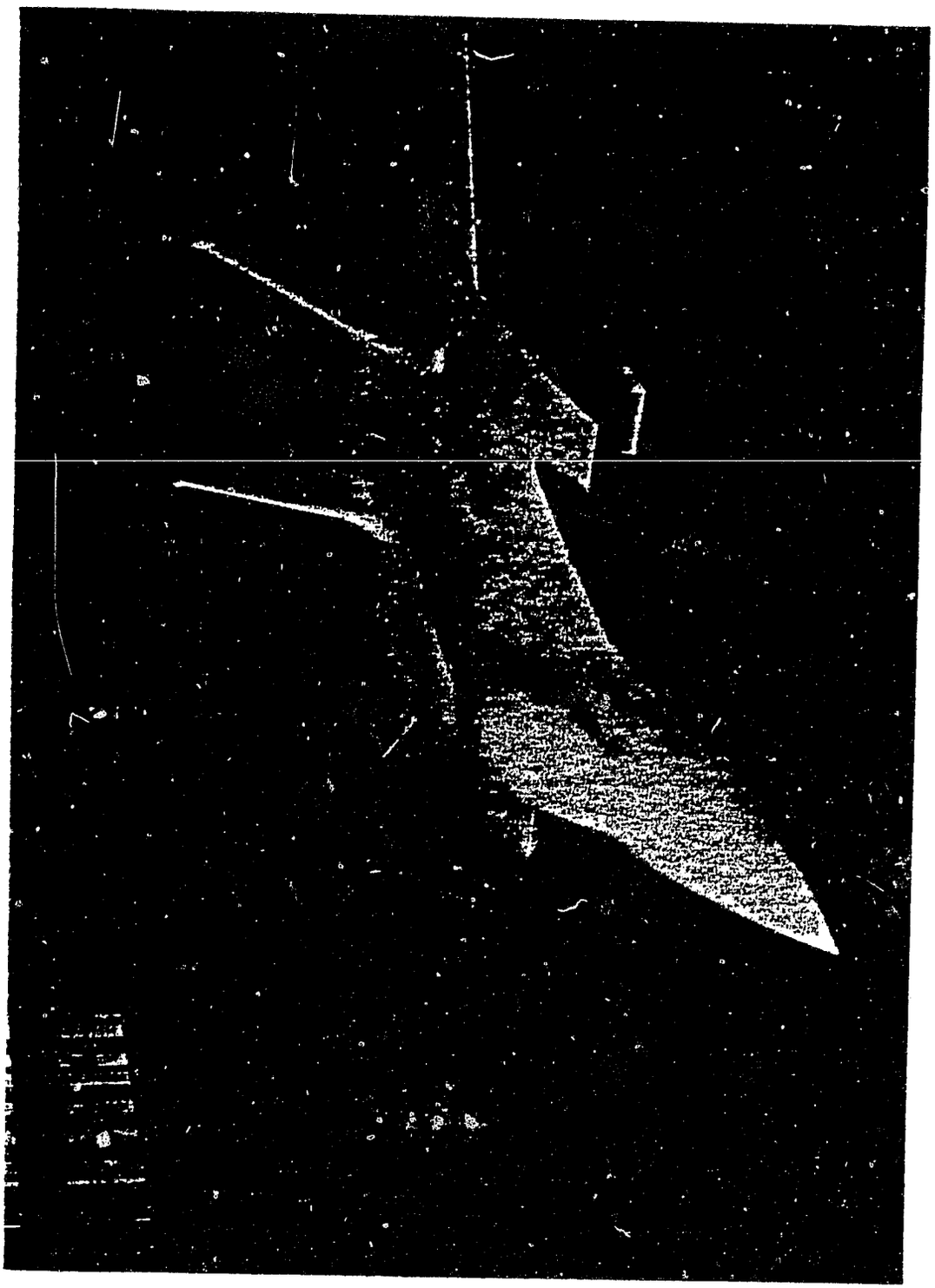

*Figure 13. 623 V/STOL Fighter Wind Tunnel Model*

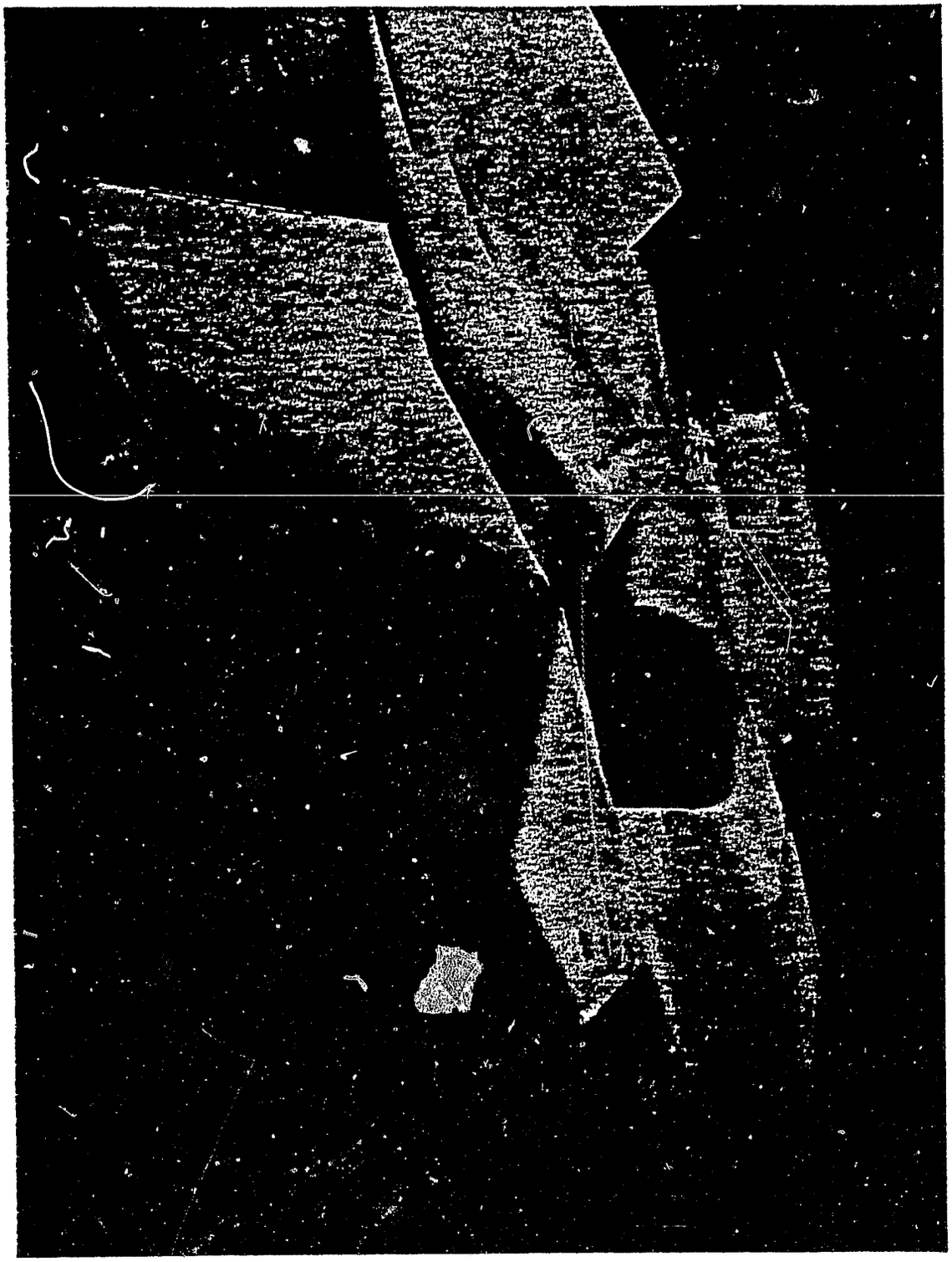

*Figure 14. 623 Model ADEN Thrust Deflector Nozzle*

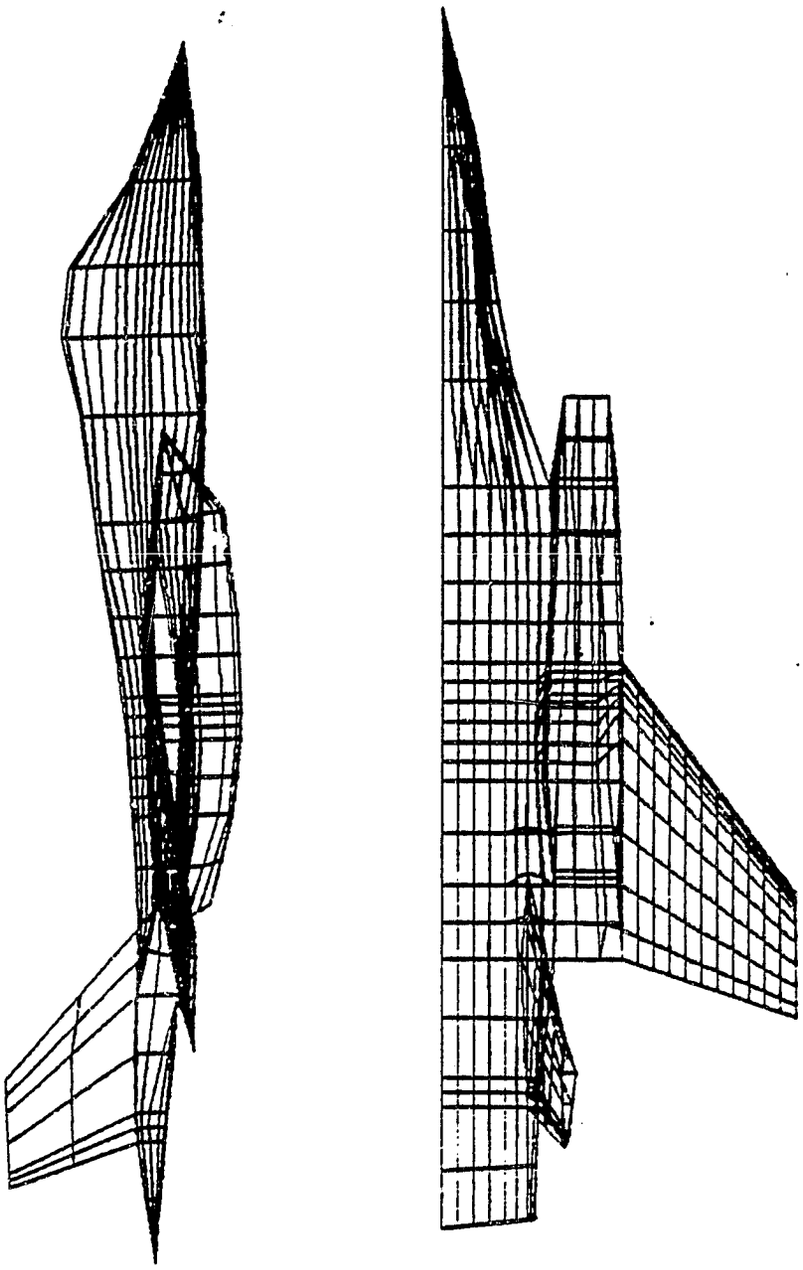

*Figure 15. Paneled 623 V/STOL Fighter Model*

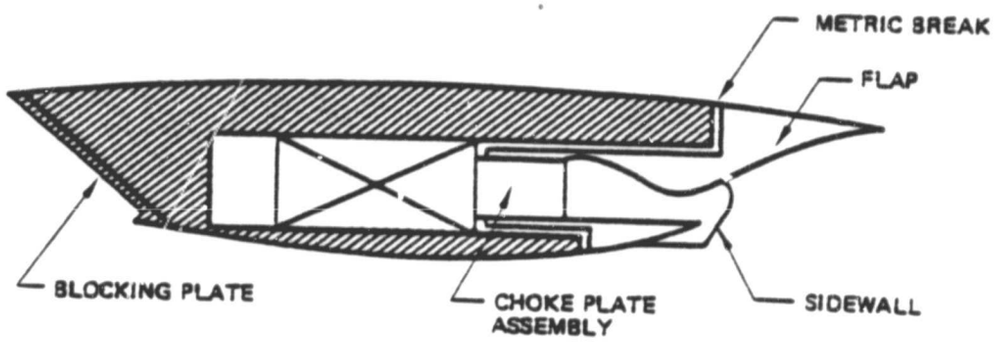


*Figure 16. Internal Geometry of the ADEN Nozzle*

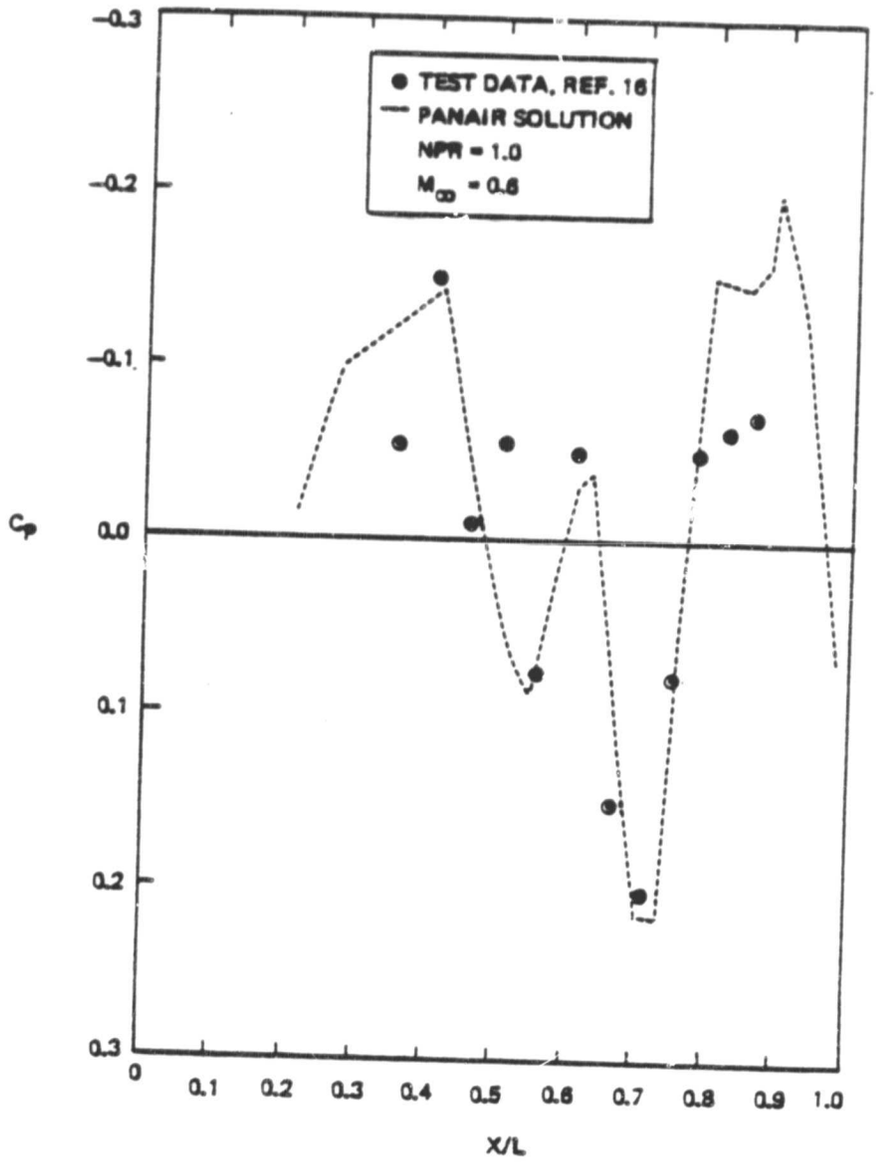


*Figure 17. Pressure Distribution on 623 Model Fuselage Upper Surface at y = 0.11 b/2 for No Flow Nozzle*

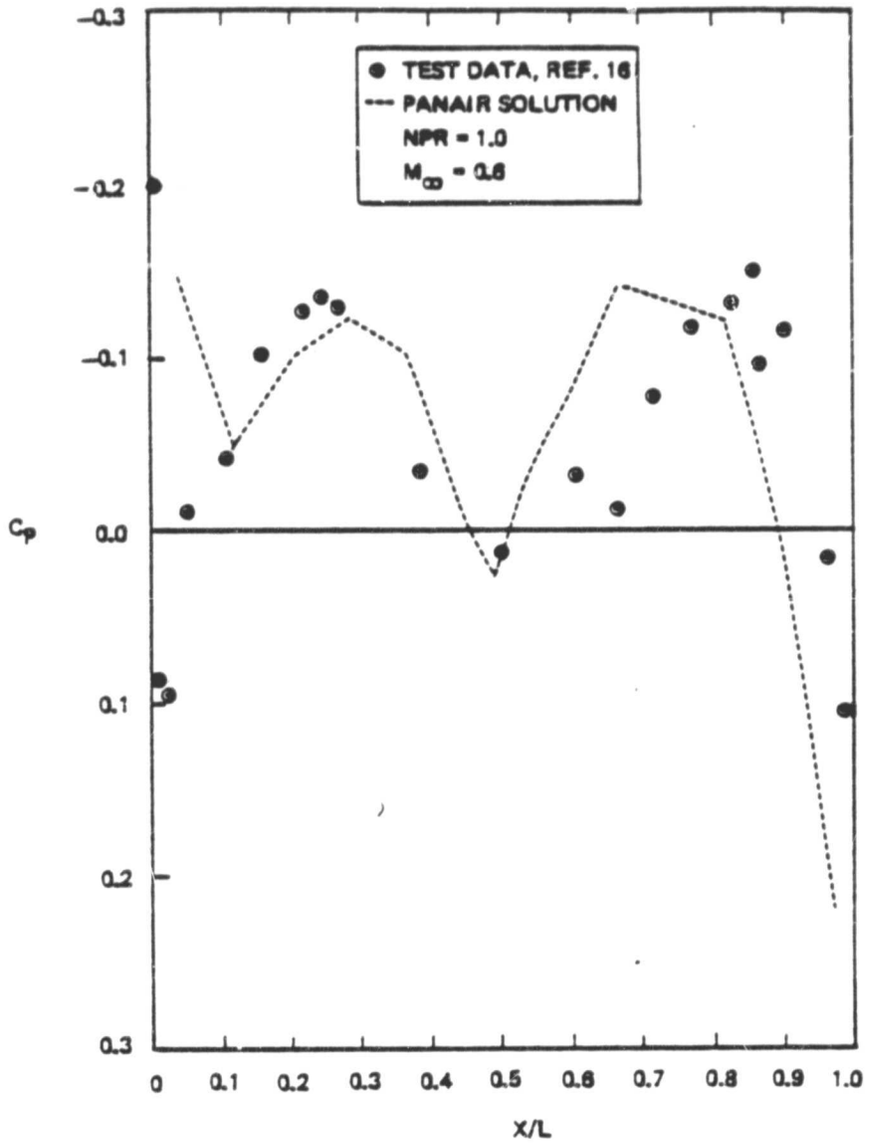


*Figure 18. Pressure Distribution on 623 Model Nacelle Upper Surface at y = 0.41 b/2 for No Flow Nozzle*

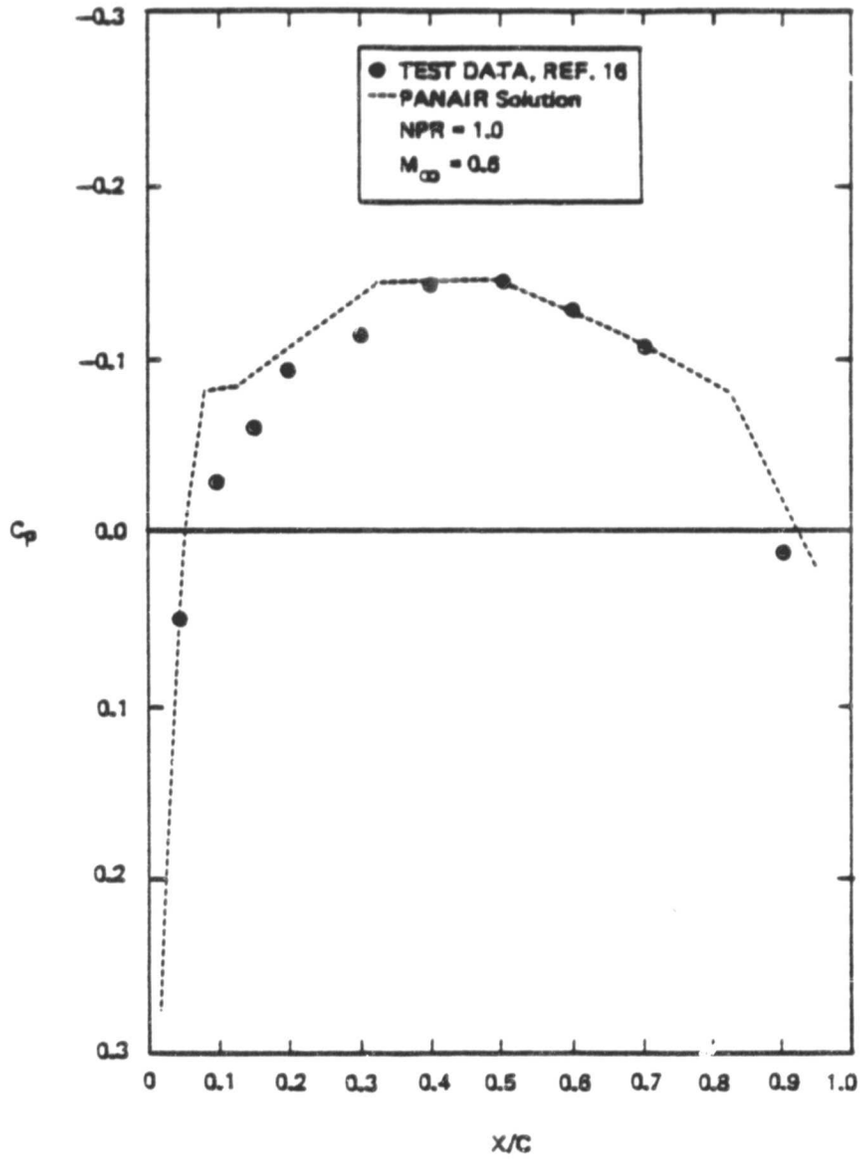


*Figure 19. Pressure Distribution on 623 Model Wing Upper Surface at y = 0.76 b/2 for No Flow Nozzle*

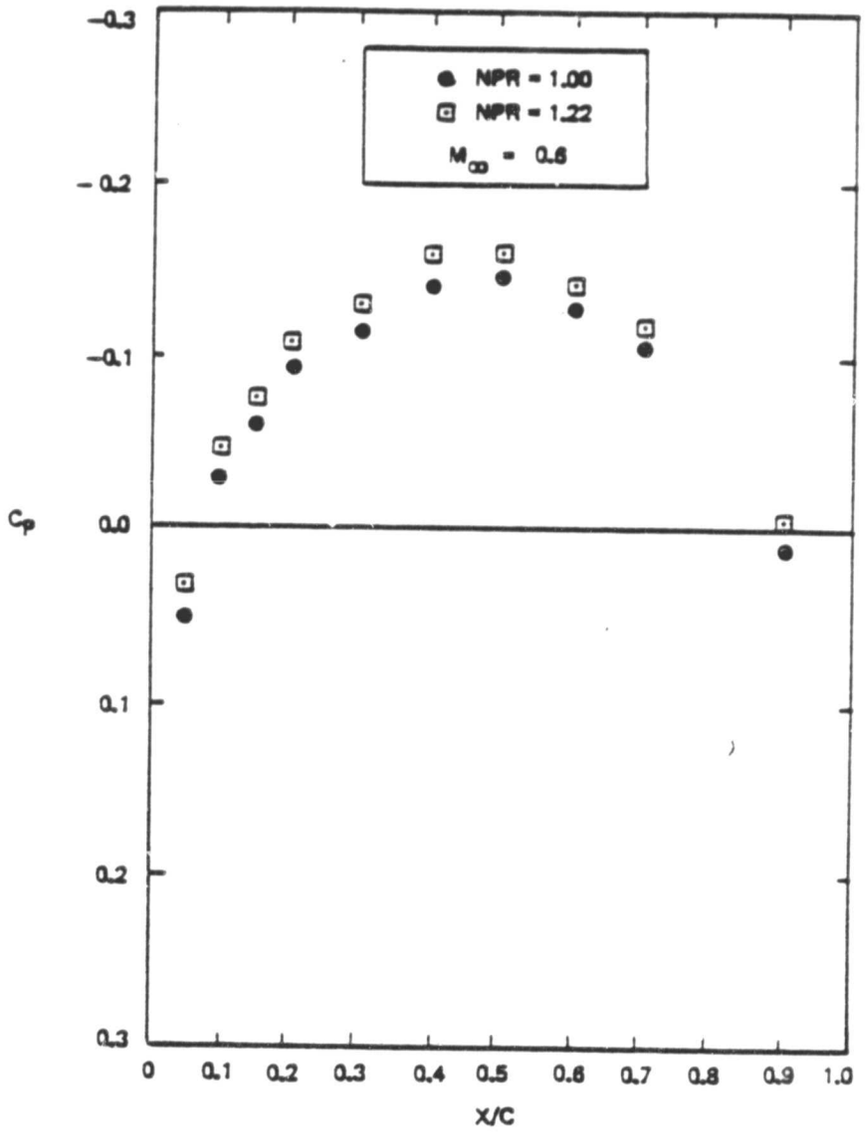


*Figure 20. Comparison of Experimental Data, Reference 16, On Wing Upper Surface for Plume and No Plume Condition*

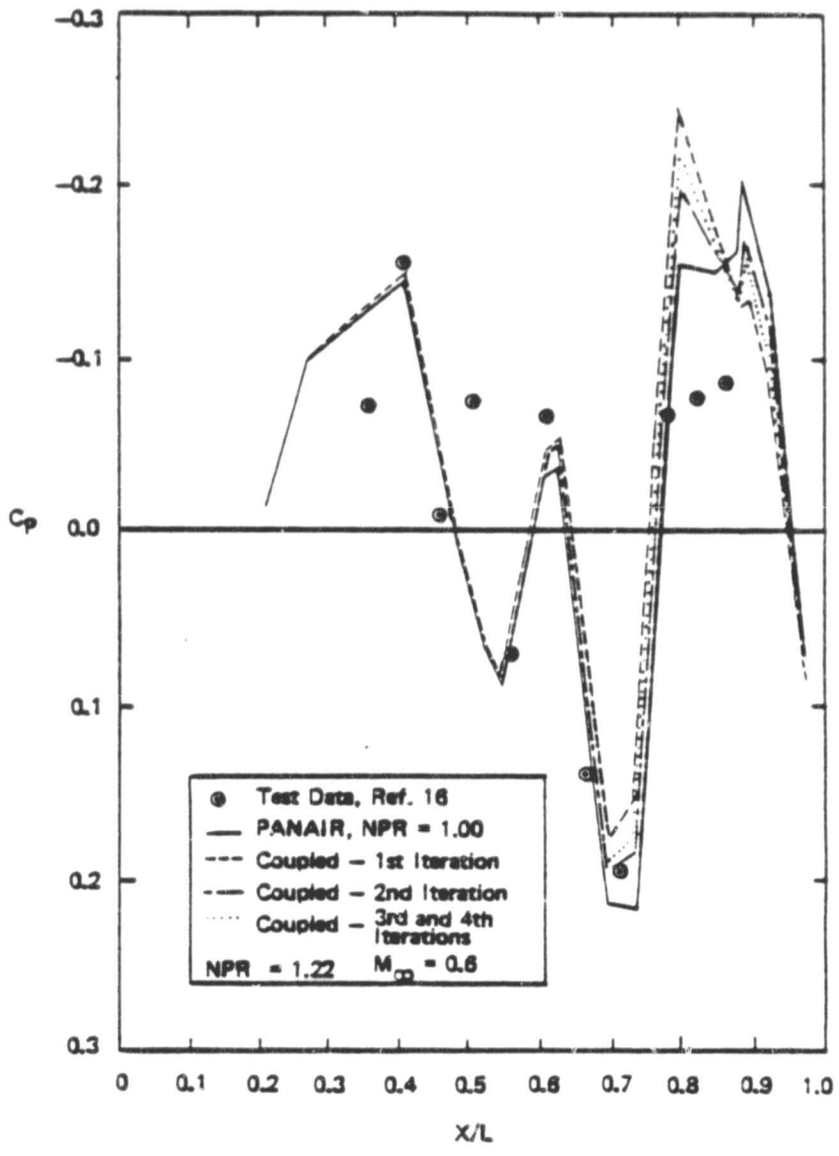


*Figure 21. Pressure Distribution on Fuselage Upper Surface at y = 0.11 b/2 for Flow Through Nacelle*

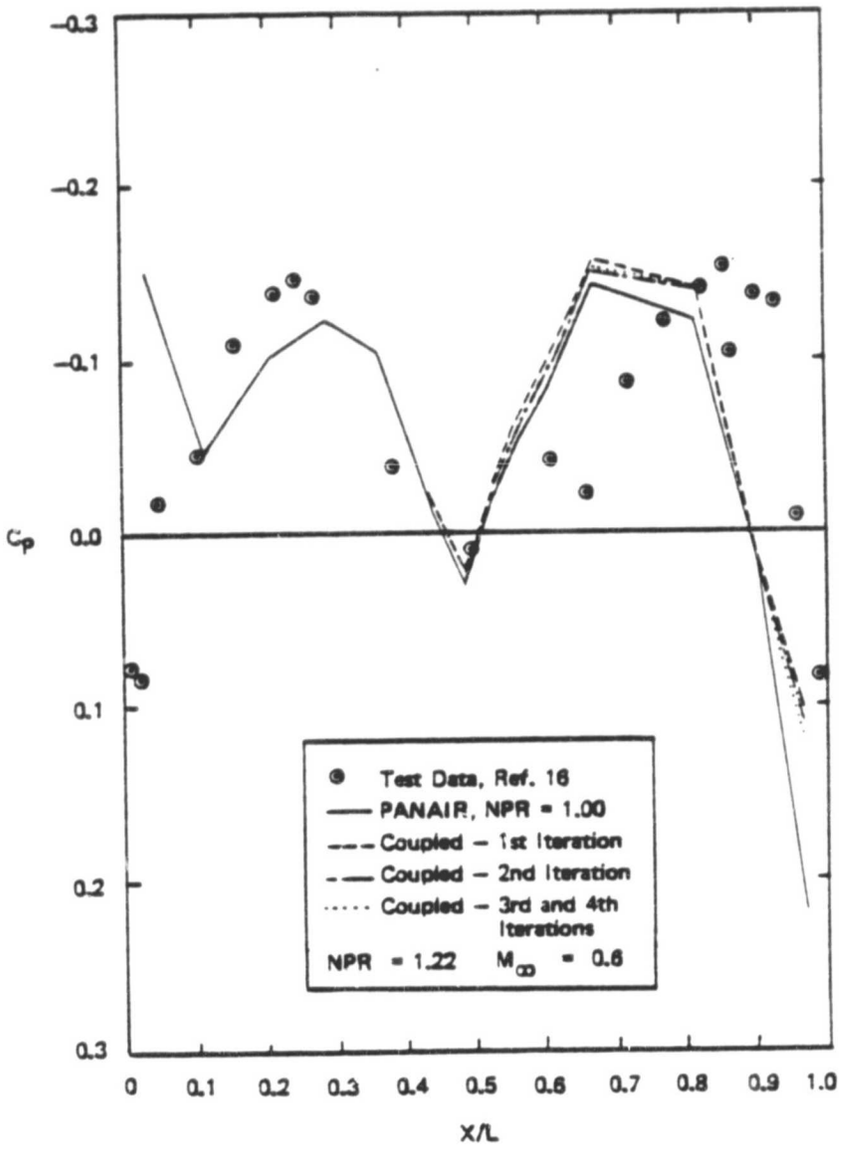


*Figure 22. Pressure Distribution on Nacelle Upper Surface at y = 0.41 b/2 for Flow Through Nacelle*

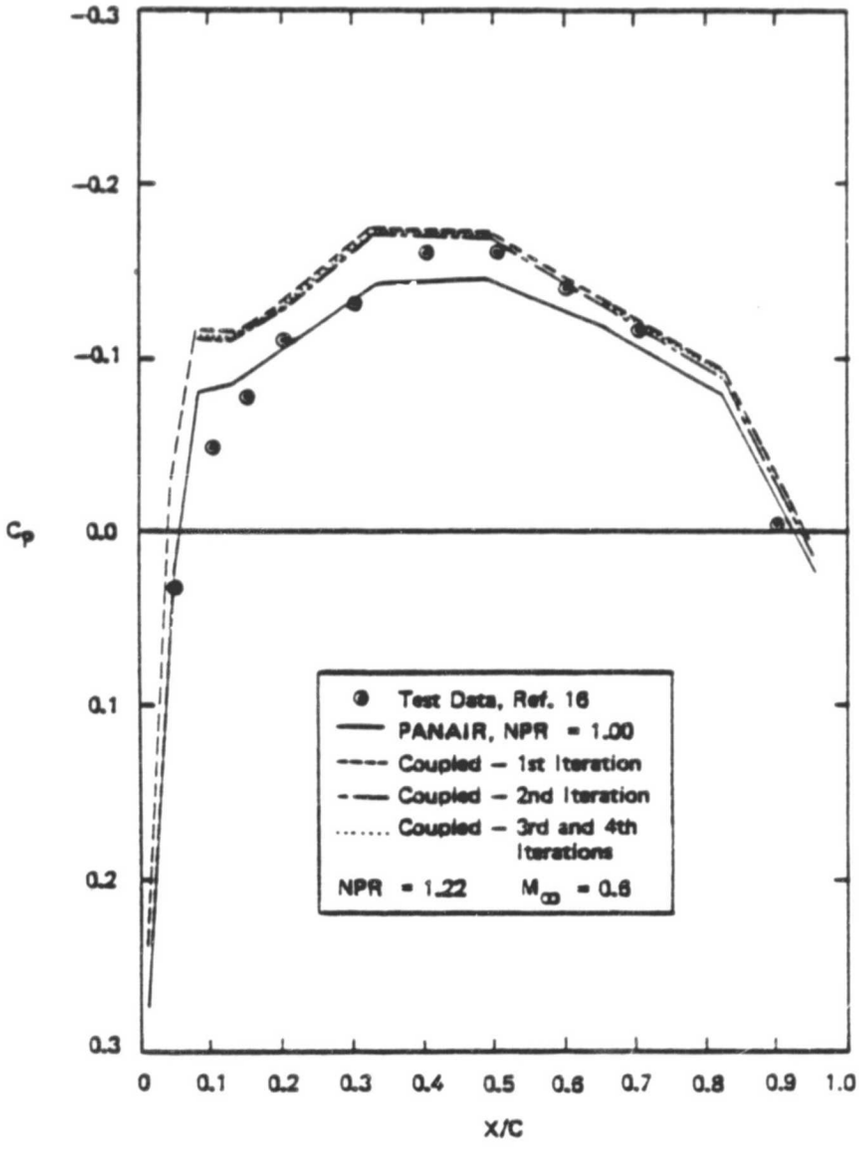


*Figure 23. Pressure Distribution on Wing Upper Surface at y = 0.76 b/2 for Flow Through Nacelle*

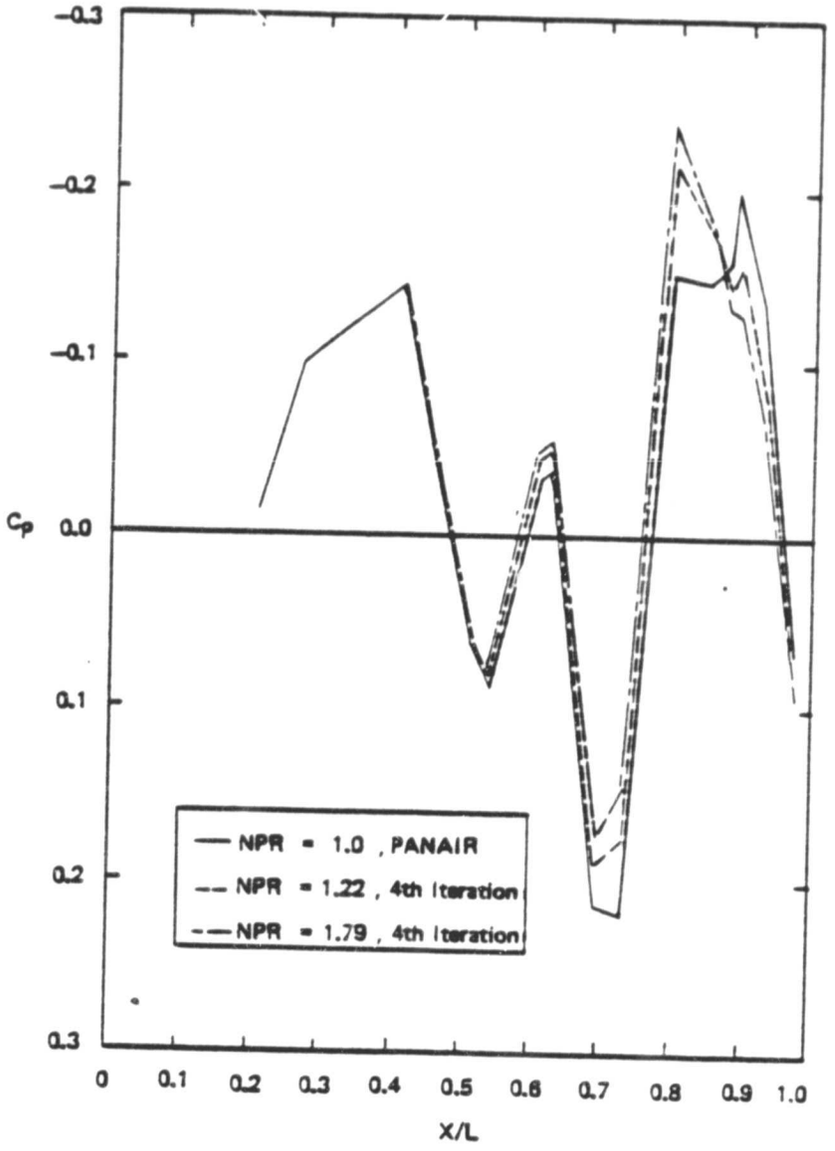


*Figure 24. Effect of Nozzle Flow Conditons on the Fuselage Pressure Distribution*

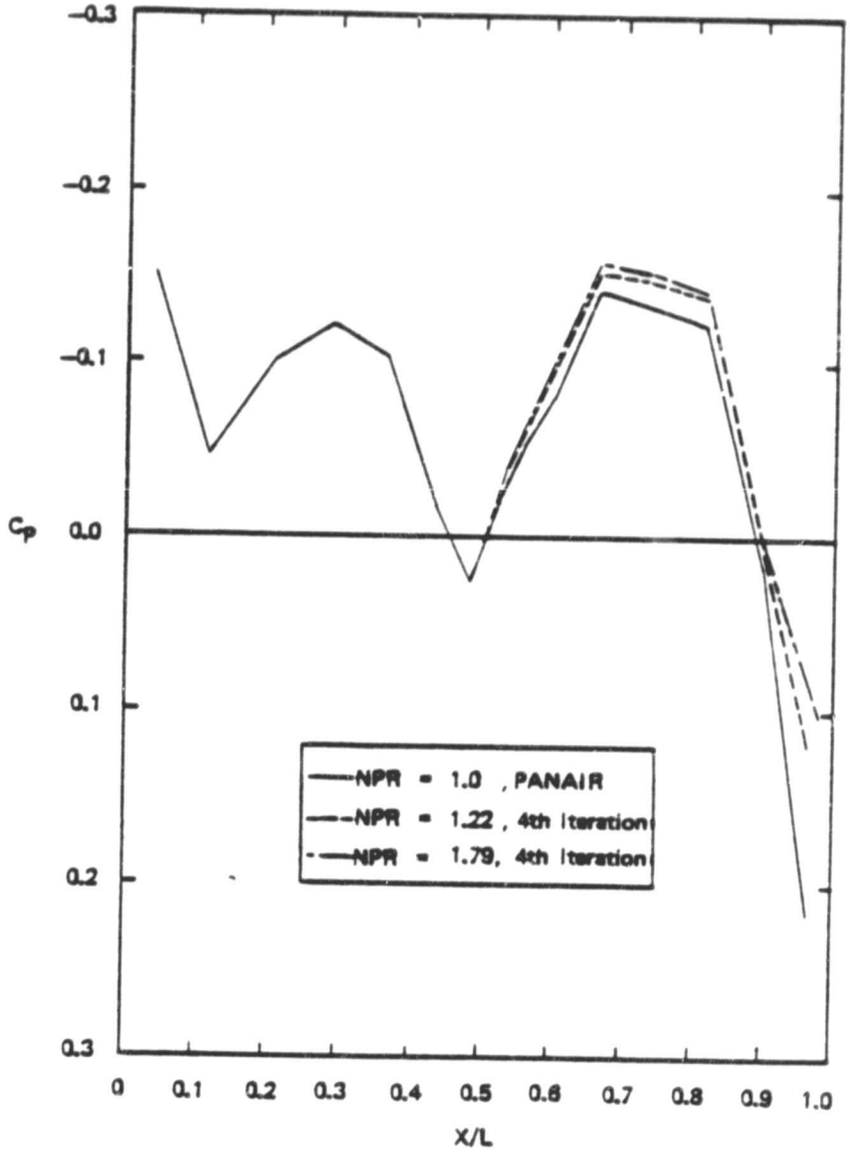


*Figure 25. Effect of Nozzle Flow Conditons on the Nacelle Pressure Distribution*

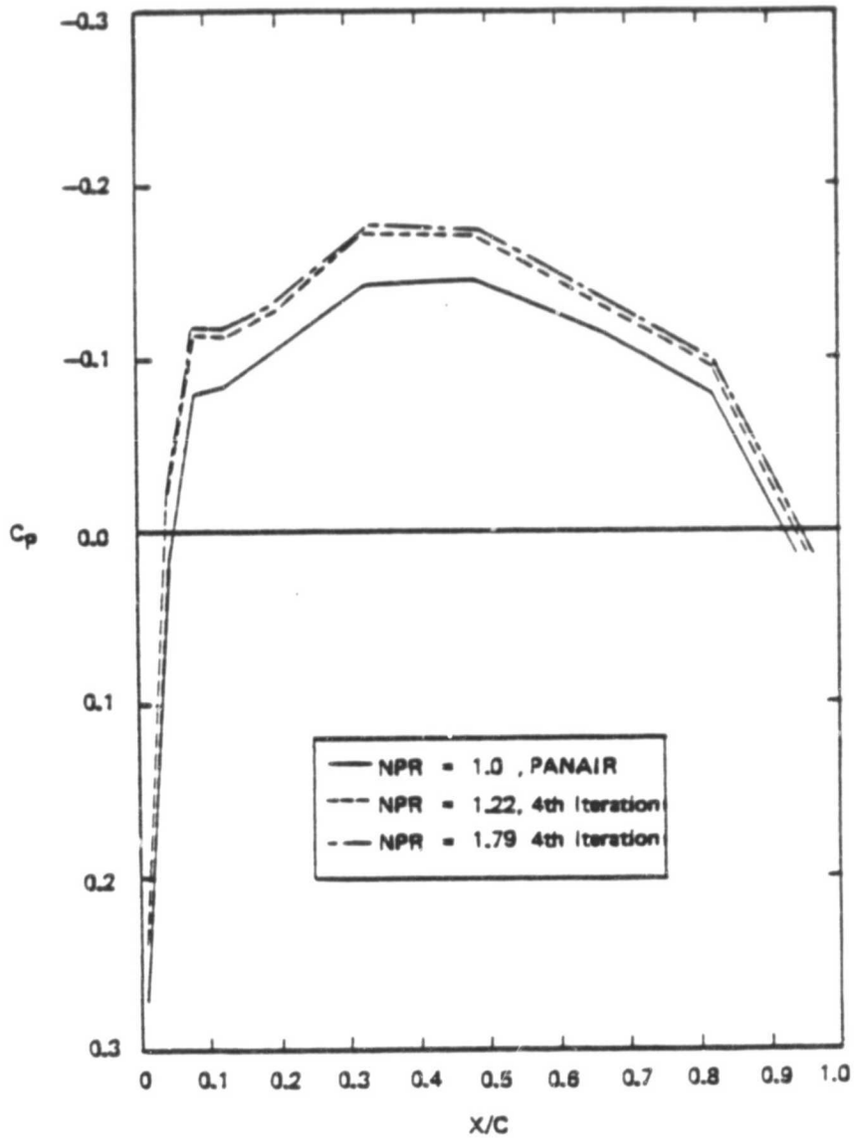


*Figure 26. Effect of Nozzle Flow Conditions on the Wing Pressure Distribution*